

This discussion paper is/has been under review for the journal Atmospheric Chemistry and Physics (ACP). Please refer to the corresponding final paper in ACP if available.

# The impact of snow nitrate photolysis on boundary layer chemistry and the recycling and redistribution of reactive nitrogen across Antarctica in a global chemical transport model

M. C. Zatko<sup>1</sup>, L. Geng<sup>1</sup>, B. Alexander<sup>1</sup>, E. D. Sofen<sup>2</sup>, and K. Klein<sup>3</sup>

<sup>1</sup>Department of Atmospheric Sciences, University of Washington, Seattle, USA

<sup>2</sup>Department of Chemistry, University of York, York, UK

<sup>3</sup>Division of Glaciology, Alfred Wegener Institute Helmholtz Centre for Polar and Marine Research, Bremerhaven, Germany

Received: 19 May 2015 – Accepted: 20 June 2015 – Published: 10 July 2015

Correspondence to: B. Alexander (beckya@uw.edu)

Published by Copernicus Publications on behalf of the European Geosciences Union.

ACPD

15, 18963–19015, 2015

The impact of snow nitrate photolysis in Antarctica

M. C. Zatko et al.

Title Page

Abstract

Introduction

Conclusions

References

Tables

Figures

◀

▶

◀

▶

Back

Close

Full Screen / Esc

Printer-friendly Version

Interactive Discussion



## Abstract

The formation and recycling of reactive nitrogen ( $\text{NO}$ ,  $\text{NO}_2$ , HONO) at the air-snow interface has implications for air quality and the oxidation capacity of the atmosphere in snow-covered regions. Nitrate ( $\text{NO}_3^-$ ) photolysis in snow provides a source of oxidants (e.g., hydroxyl radical, ozone) and oxidant precursors (e.g., nitrogen oxides) to the overlying boundary layer, and disturbs the preservation of  $\text{NO}_3^-$  in ice cores. We have incorporated the photolysis of Antarctic snow  $\text{NO}_3^-$  into a global chemical transport model (GEOS-Chem) to examine the implications of snow  $\text{NO}_3^-$  photolysis for boundary layer chemistry, the recycling and redistribution of reactive nitrogen across the Antarctic continent, and the preservation of ice-core  $\text{NO}_3^-$  in Antarctic ice cores. The calculated potential flux of snow-sourced  $\text{NO}_x$  in Antarctica ( $0.5\text{--}7.8 \times 10^8 \text{ molec cm}^{-2} \text{ s}^{-1}$ ) and calculated e-folding depths of UV actinic flux in snowpack (24–69 cm) are comparable to observations. Snow-sourced  $\text{NO}_x$  increases mean austral summer boundary layer mixing ratios of total nitrate ( $\text{HNO}_3 + \text{NO}_3^-$ ),  $\text{NO}_x$ , OH, and  $\text{O}_3$  in Antarctica by a factor of up to 32, 38, 7, and 2, respectively, in the model. Model results also suggest that  $\text{NO}_3^-$  can be recycled between the air and snow multiple times and that  $\text{NO}_3^-$  can remain in the snow photic zone for at least 7.5 years on the East Antarctic plateau. The fraction of photolysis-driven loss of  $\text{NO}_3^-$  from the snow is  $\sim 0.99$  on the East Antarctic plateau, while areas of wind convergence (e.g., over the Ronne Ice Shelf) have a net gain of  $\text{NO}_3^-$  due to redistribution of snow-sourced reactive nitrogen across the Antarctic continent. The modeled enrichment in ice-core  $\delta^{15}\text{N}(\text{NO}_3^-)$  due to photolysis-driven loss of snow  $\text{NO}_3^-$  ranges from 0 to 363‰ and the magnitudes of the spatial trends are consistent with  $\delta^{15}\text{N}(\text{NO}_3^-)$  observations, suggesting that the spatial variability in snow  $\delta^{15}\text{N}(\text{NO}_3^-)$  across the Antarctic continent is determined mainly by the degree of photolysis-driven loss of snow  $\text{NO}_3^-$ . Further, there is a strong relationship between the degree of photolysis-driven loss of snow  $\text{NO}_3^-$  and the degree of nitrogen recycling between the air and snow, suggesting that ice-core  $\delta^{15}\text{N}(\text{NO}_3^-)$  observations can be

## The impact of snow nitrate photolysis in Antarctica

M. C. Zatko et al.

[Title Page](#)

[Abstract](#)

[Introduction](#)

[Conclusions](#)

[References](#)

[Tables](#)

[Figures](#)

◀

▶

◀

▶

[Back](#)

[Close](#)

[Full Screen / Esc](#)

[Printer-friendly Version](#)

[Interactive Discussion](#)



used to assess the degree of nitrogen recycling and loss over much of Antarctica and aid in the interpretation of ice-core  $\text{NO}_3^-$  in terms of past atmospheric variability of reactive nitrogen.

## 1 Introduction

- 5 Nitrogen oxides ( $\text{NO}_x = \text{NO} + \text{NO}_2$ ) emitted from fossil fuel combustion, biomass burning, soil microbial activity, and lightning have adverse respiratory effects, contribute to the formation of atmospheric acidity, and are a key ingredient in tropospheric oxidant cycling leading to the formation of ground-level ozone ( $\text{O}_3$ ). Ozone also has adverse respiratory effects, is an effective greenhouse gas (UNEP, 2011), and its photolysis
- 10 dominants hydroxyl radical ( $\text{OH}$ ) production in much of the troposphere (Thompson, 1992). Oxidation to form nitrate ( $\text{HNO}_3/\text{NO}_3^-$ ) is the main sink for  $\text{NO}_x$  in the troposphere (Logan, 1983), and the lifetime of  $\text{NO}_x$  against oxidation to nitrate is on the order of one day (Levy et al., 1999).  $\text{NO}_3^-$  is lost from the atmosphere through dry and wet deposition to the Earth's surface, and has an atmospheric lifetime on the order
- 15 of several days (Logan, 1983). In Antarctica,  $\text{NO}_3^-$  deposited to the snowpack originates from both the troposphere (e.g., long-range transport) (Lee et al., 2014) and stratosphere (Frey et al., 2009; Savarino et al., 2007). In snow-covered regions, the deposition of  $\text{NO}_3^-$  is not a permanent sink for  $\text{NO}_x$ , as the photolysis of snow  $\text{NO}_3^-$  re-cycles reactive nitrogen ( $\text{N}_r = \text{NO}_x, \text{HONO}$ ) back to the atmosphere, with implications
- 20 for other oxidants such as  $\text{OH}$  and ozone (Domine and Shepson, 2002).

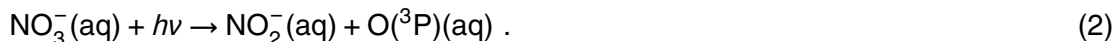
Snow photochemistry significantly influences boundary layer chemistry and plays an important role in oxidant production and cycling, especially in pristine regions, such as Antarctica (Bloss et al., 2007; Chen et al., 2004; Grannas et al., 2007; Helmhig et al., 2008). Snow photochemistry may have more widespread impacts since up to 40 % of land on Earth is snow-covered at a given time (Grannas et al., 2007).  $\text{NO}_3^-$  is not the only photochemically-active species in snow. The photolysis of nitrite ( $\text{NO}_2^-$ ) in snow and the photolysis of snow-sourced formaldehyde ( $\text{CH}_2\text{O}$ ), nitrous acid ( $\text{HONO}$ ), and

<a href="#">Title Page</a>	
<a href="#">Abstract</a>	<a href="#">Introduction</a>
<a href="#">Conclusions</a>	<a href="#">References</a>
<a href="#">Tables</a>	<a href="#">Figures</a>
<a href="#">◀</a>	<a href="#">▶</a>
<a href="#">◀</a>	<a href="#">▶</a>
<a href="#">Back</a>	<a href="#">Close</a>
<a href="#">Full Screen / Esc</a>	
<a href="#">Printer-friendly Version</a>	
<a href="#">Interactive Discussion</a>	



hydrogen peroxide ( $\text{H}_2\text{O}_2$ ) provide additional sources of  $\text{N}_\text{r}$  and  $\text{OH}$  to the boundary layer. Bromine ( $\text{Br}_2$ ) is also produced in the snow via reactions involving bromide ( $\text{Br}^-$ ), photochemically-active species (e.g.,  $\text{NO}_3^-$ ), and photochemically-produced species (e.g.,  $\text{OH}$ ) within snow grains (Pratt et al., 2013).

In snow,  $\text{NO}_3^-$  photolysis likely occurs in the liquid-like region (LLR) on the surface of ice grains, in cracks between ice grains, or in brine pockets embedded within ice grains (Domine et al., 2013). There are two channels for  $\text{NO}_3^-$  photolysis at wavelengths ( $\lambda$ ) = 290–345 nm. In the aqueous phase,  $\text{NO}_3^-$  can photolyze to produce  $\text{NO}_2$  and  $\text{OH}$  (Eq. 1), or produce  $\text{NO}_2^-$  and  $\text{O}^{(3)\text{P}}$  (Eq. 2), but Eq. (1) is the dominant pathway (Grannas et al., 2007; Mack and Bolton, 1999; Meusinger et al., 2014).



The aqueous phase  $\text{NO}_2$  produced in Eq. (1) is partially transferred to the gas phase,  $\text{NO}_2(\text{g})$ , during transport from the LLR to the interstitial air (Boxe et al., 2005). The quantum yield ( $\phi$ ) in Eq. (1) is strongly influenced by the location of  $\text{NO}_3^-$  in an ice grain. Chu and Anastasio (2003) froze  $\text{NO}_3^-$ -doped water in the lab and measured the quantum yield for Eq. (1) ( $3 \times 10^{-3}$  molec photon $^{-1}$  at  $T = 253\text{K}$ ) as frozen ice grains were exposed to ultraviolet (UV) radiation. Zhu et al. (2010) deposited  $\text{HNO}_3$  on an ice film and measured  $\phi$  for Eq. (1) ( $0.6$  molec photon $^{-1}$  at  $T = 253\text{K}$ ), as the frozen surface was irradiated with UV radiation. In a recent study by Meusinger et al. (2014),  $\phi = 0.003\text{--}0.44$  molec photon $^{-1}$  for Eq. (1) which spans the range of previously reported quantum yields. Results from Meusinger et al. (2014) suggest that  $\phi$  is dependent on the length of time that snow was exposed to UV radiation, as well as and the location of  $\text{NO}_3^-$  in the ice grain. Meusinger et al. (2014) suggest that two photochemical domains of  $\text{NO}_3^-$  exist: photolabile  $\text{NO}_3^-$  and  $\text{NO}_3^-$  buried within the ice grain. The  $\text{NO}_x$  produced from the photolysis of photolabile  $\text{NO}_3^-$  can escape the ice grain, while the  $\text{NO}_x$  produced from the photolysis of buried  $\text{NO}_3^-$  is likely to undergo recom-

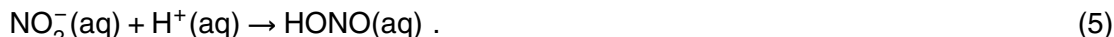
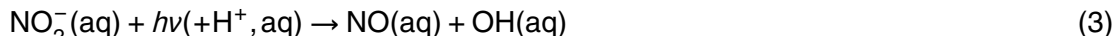
<a href="#">Title Page</a>	
<a href="#">Abstract</a>	<a href="#">Introduction</a>
<a href="#">Conclusions</a>	<a href="#">References</a>
<a href="#">Tables</a>	<a href="#">Figures</a>
<a href="#"></a>	<a href="#"></a>
<a href="#"></a>	<a href="#"></a>
<a href="#">Full Screen / Esc</a>	
<a href="#">Printer-friendly Version</a>	
<a href="#">Interactive Discussion</a>	



[Title Page](#)[Abstract](#)[Introduction](#)[Conclusions](#)[References](#)[Tables](#)[Figures](#)[◀](#)[▶](#)[◀](#)[▶](#)[Back](#)[Close](#)[Full Screen / Esc](#)[Printer-friendly Version](#)[Interactive Discussion](#)

bination chemistry within the snow grain, thus lowering the quantum yield of  $\text{NO}_x$  for  $\text{NO}_3^-$  photolysis.

The  $\text{NO}_2^-$  produced in Eq. (2) is quickly photolyzed at longer wavelengths ( $\lambda = 290\text{--}390\text{ nm}$ ) in the LLR or can react with OH or  $\text{H}^+$  in the LLR to produce  $\text{N}_r$  (Grannas et al., 2007):  
<sup>5</sup>



$\text{HONO}$  produced in Eq. (5) can rapidly photolyze to produce NO and OH in the interstitial air or the atmospheric boundary layer (Anastasio and Chu, 2009). Reactions involving  $\text{NO}_2^-$  are intermediate reactions for  $\text{NO}_3^-$  photolysis because  $\text{NO}_3^-$  photolysis is required for  $\text{NO}_2^-$  formation and the end products of Eqs. (1)–(5) are all  $\text{N}_r$ . Once emitted,  $\text{NO}_2$  and NO are efficiently transported to the overlying atmosphere via wind pumping (Zatko et al., 2013) and enter into rapid  $\text{NO}_x$ -cycling reactions. In the atmosphere,  
<sup>10</sup> the relative abundance of NO and  $\text{NO}_2$  will be determined by local atmospheric conditions, specifically oxidant concentrations (e.g.,  $\text{O}_3$ ,  $\text{HO}_2$ ,  $\text{RO}_2$ ,  $\text{BrO}$ , and  $\text{ClO}$ ) (Frey et al., 2013). The snow-sourced  $\text{NO}_x$  is then re-oxidized to  $\text{HNO}_3$  via Eq. (6) under sunlit conditions.  
<sup>15</sup>



$\text{HNO}_3$  produced in Eq. (6) can undergo wet or dry deposition to the snow surface (Dibb et al., 2004) within a day (Slusher et al., 2002; Wang et al., 2008). Evidence for  $\text{HNO}_3$  re-deposition is seen in the snow  $\text{NO}_3^-$  concentration profile at many polar locations, where  $\text{NO}_3^-$  concentrations are at least an order of magnitude higher in the top two centimeters (cm) of snow compared to  $\text{NO}_3^-$  concentrations below (Dibb et al.,  
<sup>20</sup> 2004; Frey et al., 2009; Mayewski and Legrand, 1990; Rothlisberger et al., 2000). Once  $\text{HNO}_3$  is deposited back to the snow, it is available for photolysis again.  $\text{NO}_3^-$  can be  
<sup>25</sup>

## The impact of snow nitrate photolysis in Antarctica

M. C. Zatko et al.

[Title Page](#)

[Abstract](#)

[Introduction](#)

[Conclusions](#)

[References](#)

[Tables](#)

[Figures](#)

◀

▶

[Back](#)

[Close](#)

[Full Screen / Esc](#)

[Printer-friendly Version](#)

[Interactive Discussion](#)



recycled multiple times between the boundary layer and the snow before burial below the photic zone (Davis et al., 2008; Erbland et al., 2015).

- The photolysis of snow  $\text{NO}_3^-$  and subsequent recycling between the air and snow disturbs the preservation of  $\text{NO}_3^-$  in polar ice sheets and hampers the interpretation of ice-core  $\text{NO}_3^-$  concentration records (Wolff et al., 2008). Such records have been sought to reconstruct the past history of the abundance of  $\text{NO}_x$  in the atmosphere (Wolff, 1995). It has also been suggested that the nitrogen ( $\delta^{15}\text{N}$ ) and oxygen ( $\Delta^{17}\text{O} = \delta^{17}\text{O} - 0.52 \times \delta^{18}\text{O}$ ) isotopic composition of ice-core  $\text{NO}_3^-$  can provide information on past variability in atmospheric  $\text{NO}_x$  sources and oxidant abundances (e.g., Alexander et al., 2004; Hastings et al., 2005). Different sources of  $\text{NO}_x$  have different  $\delta^{15}\text{N}$  signatures ( $\sim -19$  to  $25\text{\textperthousand}$ , see summary in Geng et al., 2014a), giving ice-core  $\delta^{15}\text{N}(\text{NO}_3^-)$  measurements the potential to track  $\text{NO}_x$ -source changes over time. The oxygen-17 excess of  $\text{NO}_3^-$  ( $\Delta^{17}\text{O}(\text{NO}_3^-)$ ) is determined mainly by the relative abundance of the oxidants involved in  $\text{NO}_x$  cycling and conversion of  $\text{NO}_2$  to  $\text{NO}_3^-$  (i.e.  $\text{O}_3$ ,  $\text{HO}_2$ ,  $\text{RO}_2$ ,  $\text{OH}$ ), giving ice-core  $\Delta^{17}\text{O}(\text{NO}_3^-)$  measurements the potential to track variability in the relative abundance of these oxidants over time. However, the preservation of  $\delta^{15}\text{N}(\text{NO}_3^-)$  and  $\Delta^{17}\text{O}(\text{NO}_3^-)$  in ice cores can also be influenced by post-depositional processing of snow  $\text{NO}_3^-$  initiated by photolysis. In this study we focus on the impact of snow nitrate photolysis on ice-core  $\delta^{15}\text{N}(\text{NO}_3^-)$ .
- Ice-core  $\delta^{15}\text{N}(\text{NO}_3^-)$  values will be altered if there is photolysis-driven loss of  $\text{NO}_3^-$  from the snow when snow-sourced  $\text{NO}_x$  is transported away from the site of primary deposition. Nitrate photolysis in snow is associated with a large fractionation constant ( $\varepsilon$ ) of  $-47.9\text{\textperthousand}$  (Berhanu et al., 2014), providing the boundary layer with a source of  $\text{NO}_x$  that is highly depleted in  $\delta^{15}\text{N}$ , leaving highly enriched  $\delta^{15}\text{N}(\text{NO}_3^-)$  in the snow.
- In the Weddell Sea, atmospheric  $\delta^{15}\text{N}(\text{NO}_3^-)$  values are as low as  $-40\text{\textperthousand}$ , indicating transport of snow-sourced  $\text{NO}_x$  from the continental interior (Morin et al., 2009), while on the East Antarctica plateau, snow  $\delta^{15}\text{N}(\text{NO}_3^-)$  up to  $480\text{\textperthousand}$  has been reported (Blunier et al., 2005; Erbland et al., 2013; Frey et al., 2009; Shi et al., 2014), indicating net

loss of  $\text{NO}_3^-$  driven by photolysis. If snow-sourced  $\text{NO}_x$  is simply re-deposited back to the snow surface at the site of emission, a vertical profile in  $\delta^{15}\text{N}(\text{NO}_3^-)$  within the snow photic zone will develop due to vertical redistribution of  $\text{NO}_3^-$  (Erblad et al., 2013; Frey et al., 2009); however, the depth-integrated  $\delta^{15}\text{N}(\text{NO}_3^-)$  will not be impacted, even with active photolysis-driven recycling between the atmosphere and the snow. Enrichment in  $\delta^{15}\text{N}(\text{NO}_3^-)$  in ice cores requires photolysis-driven loss from snow combined with atmospheric transport of the resulting  $\text{NO}_x$ . In addition to photolysis, ice-core  $\delta^{15}\text{N}(\text{NO}_3^-)$  values are also influenced by evaporation of  $\text{HNO}_3$  (Mulvaney et al., 1998) from snow and by atmospheric processing, such as  $\text{NO}_x$  cycling (Freyer et al., 1993) and gas-particle partitioning (Heaton et al., 1997; Geng et al., 2014a); however, these impose a fractionation in  $\delta^{15}\text{N}(\text{NO}_3^-)$  at least an order of magnitude smaller than photolysis, and are thus not able to explain the large enrichments in snow  $\delta^{15}\text{N}(\text{NO}_3^-)$  observed on the East Antarctic plateau (Blunier et al., 2005; Erblad et al., 2013; Frey et al., 2009; Shi et al., 2014).

Here we incorporate a snowpack actinic flux parameterization used to calculate the photolysis of snow  $\text{NO}_3^-$  into a global chemical transport model. This modeling framework is used to evaluate the impact of a snow-sourced  $\text{NO}_x$  and the associated reactive nitrogen recycling and redistribution on boundary layer chemistry and the preservation of ice-core  $\text{NO}_3^-$  across the Antarctic continent. A major advantage of using a global chemical transport model framework is the ability to examine the redistribution and loss of reactive nitrogen across large spatial scales, such as the Antarctic continent, due to photolysis loss of snow  $\text{NO}_3^-$ . Section 2 describes the inclusion of a snowpack actinic flux parameterization and  $\text{NO}_3^-$  photolysis into a global chemical transport model, GEOS-Chem. Section 3 explores the implications of photolysis-driven reactive nitrogen recycling and redistribution for boundary layer chemistry and  $\text{NO}_3^-$  preservation in ice cores. We end by using our model sensitivity studies to highlight the largest uncertainties in our ability to model these processes as a guide for future laboratory and field studies.

[Title Page](#)[Abstract](#)[Introduction](#)[Conclusions](#)[References](#)[Tables](#)[Figures](#)[◀](#)[▶](#)[◀](#)[▶](#)[Back](#)[Close](#)[Full Screen / Esc](#)[Printer-friendly Version](#)[Interactive Discussion](#)

## 2 Methods

### 2.1 Incorporating snow $\text{NO}_3^-$ photolysis into a global chemical transport model

Table 1 provides a glossary of the variables used throughout this paper.

#### 2.1.1 Global chemical transport model description

- 5 GEOS-Chem is a global 3-dimensional (3-D) model of coupled aerosol-oxidant chemistry with detailed  $\text{HO}_x\text{-NO}_x\text{-VOC-O}_3\text{-BrO}_x$  tropospheric chemistry originally described in Bey et al. (2001). The model uses assimilated meteorological data from the NASA Goddard Earth Observing System (GEOS-5) including winds, convective mass fluxes, boundary layer depths, temperature, precipitation, and surface properties. Meteorological data have 6 h temporal resolution (3 h for surface variables and mixing depths).  
10 The direct and diffuse downwelling surface irradiance and photolysis frequencies are calculated using the Fast-JX radiative transfer module (Wild et al., 2000; Bian and Prather, 2002; Mao et al., 2010). In GEOS-Chem, aerosols can be wet deposited via scavenging in convective updrafts and rainout from convective anvils and large-scale  
15 precipitation (Liu et al., 2001). The wet deposition scheme for gases is described by Amos et al. (2012) and the scavenging of aerosol by snow and cold/mixed precipitation is described by Wang et al. (2011). Dry-deposition velocities for coarse mode aerosols (radii between 1–10 mm) are calculated based on aerosol size and hydroscopic growth as described in Zhang et al. (2001). Aerosol deposition to snow and ice surfaces is  
20 described by Fisher et al. (2011). For smaller aerosols (radii less than 1  $\mu\text{m}$ ), dry deposition velocities are calculated with a standard resistance-in-series scheme (Wang et al., 1998; Wesely, 1989).

Anthropogenic  $\text{NO}_x$  emissions are from the EDGAR 3.2-FT2000 global inventory for the year 2000 (Oliver et al., 2005), scaled by country on the basis of energy statistics  
25 as described by van Donkelaar et al. (2008). The monthly inventory of emissions from biomass burning are from the Global Fire Emissions Database (GFED2) (van der Werf

<a href="#">Title Page</a>	
<a href="#">Abstract</a>	<a href="#">Introduction</a>
<a href="#">Conclusions</a>	<a href="#">References</a>
<a href="#">Tables</a>	<a href="#">Figures</a>
<a href="#">◀</a>	<a href="#">▶</a>
<a href="#">◀</a>	<a href="#">▶</a>
<a href="#">Back</a>	<a href="#">Close</a>
<a href="#">Full Screen / Esc</a>	
<a href="#">Printer-friendly Version</a>	
<a href="#">Interactive Discussion</a>	



et al., 2009). Soil  $\text{NO}_x$  emissions are computed using a parameterization described in Hudman et al. (2012), which is a function of vegetation type, temperature, soil moisture, precipitation, and fertilizer emissions. Emissions of  $\text{NO}_x$  from lightning are linked to deep convection following the parameterization of Price and Rind (1992) and are scaled globally as described by Murray et al. (2012) to match OTD/LIS climatological observations of lightning flashes. The stratospheric source of  $\text{NO}_y$  ( $= \text{NO}_x + \text{HNO}_3$ ) utilizes monthly climatological 3-D production and loss rates from the Global Modeling Initiative (GMI) model (Allen et al., 2010), which captures the formation of the polar vortex and PSC sedimentation (Murray et al., 2012).

For this work, GEOS-Chem version v9-01-01 was run at  $2^\circ \times 2.5^\circ$  horizontal resolution with 72 hybrid vertical levels using GEOS-5 meteorology from May 2009 to May 2010. The model was spun up for six months prior to May 2008. There are no subsurface (snow) layers in GEOS-Chem and the three lowest vertical levels are each roughly 100 m in height above Antarctica. The boundary layer in GEOS-Chem is calculated using a parameterization involving the bulk Richardson number with surface friction, a turbulent velocity scale, and non-local fluxes of heat and moisture (Hotslag and Boville, 1993). The mixing of emissions, dry deposition, and concentrations of individual species within the boundary layer are determined by static instability. In a stable boundary layer, the local scheme based on eddy diffusivity-theory is used, and the mixing is weak. In an unstable boundary layer, boundary layer mixing is triggered by large eddies. Average boundary layer mixing ratios (ppbv) of species reported in this study (e.g.,  $\text{NO}_3^-$ ,  $\text{NO}_x$ ,  $\text{OH}$ ,  $\text{O}_3$ ) are mixing ratios in the lowest vertical grid box. The calculated boundary layer mixing ratios are insensitive to whether the average mixing ratios in the lowest grid box (total height  $\sim 100$  m) or the three lowest grid boxes (total height  $\sim 300$  m) are used.

Figure 1 illustrates the nitrogen recycling associated with snow  $\text{NO}_3^-$  photolysis as included in the model. The total flux of snow-sourced  $\text{NO}_x$  from the snow,  $F_{\text{NO}_x}$  ( $\text{mole} \text{ cm}^{-2} \text{ s}^{-1}$ ), is calculated using the wavelength-dependent absorption cross-section for  $\text{NO}_3^-$  photolysis ( $\sigma_{\text{NO}_3^-}$ ,  $\text{cm}^2$ ), the quantum yield for  $\text{NO}_3^-$  photolysis

[Title Page](#)[Abstract](#)[Introduction](#)[Conclusions](#)[References](#)[Tables](#)[Figures](#)[◀](#)[▶](#)[Back](#)[Close](#)[Full Screen / Esc](#)[Printer-friendly Version](#)[Interactive Discussion](#)

( $\phi$ , molec photon $^{-1}$ ), the depth- and wavelength-integrated actinic flux in the snow photic zone ( $I$ , photons cm $^{-2}$  s $^{-1}$  nm $^{-1}$ ), and the average NO $_3^-$  concentration ([NO $_3^-$ ], molec cm $^{-3}$ ) over the depth of integration.  $F_{\text{NO}_x}$  is calculated in Eq. (7) and converted into units of ng N m $^{-2}$  year $^{-1}$  in Eqs. (8), (10) and (11) below.

$$F_{\text{NO}_x} = \int_{\lambda_0}^{\lambda_1} \int_{z_0}^{z_{3e}} \sigma_{\text{NO}_3^-}(\lambda) \cdot \phi \cdot I(\lambda, z) \cdot [\text{NO}_3^-] d\lambda dz . \quad (7)$$

In Eq. (7),  $\sigma_{\text{NO}_3^-}$  is from Burley and Johnston (1992),  $\phi$  is from Chu and Anastasio (2003) and Zhu et al. (2010), and the actinic flux ( $I$ ) has been integrated from the snow surface ( $z_0$ ) to the depth of the photic zone ( $z_{3e}$ ). The snow photic zone is defined as three times the e-folding depth of ultraviolet (UV) actinic flux in snow ( $z_{3e}$ ), where 1 e-folding depth is  $z_e$ . Below  $z_{3e}$ , more than 95 % of the radiation has been attenuated and minimal photochemistry occurs. The flux of snow-sourced NO $_x$  is integrated over several ultraviolet wavelength bands (298–307, 307–312, 312–320, 320–345 nm), which are then summed to calculate total  $F_{\text{NO}_x}$  from the photolysis of snow NO $_3^-$  between  $\lambda = 298$ –345 nm. We assume that all NO $_x$  formed in Eq. (7) is immediately desorbed into the gas-phase and transported to the overlying boundary layer.

## 2.1.2 Calculating radiative transfer in snow

A 2-stream, plane parallel snowpack actinic flux parameterization based on a 4-stream radiative transfer model (Grenfell, 1991) was developed and described in Zatko et al. (2013) and has been implemented into GEOS-Chem for the purposes of this study. The parameterization is simple, broadly applicable, and allows for variation in snow and sky properties (e.g., solar zenith angle, cloud fraction) over time. Ice grains are assumed to be spherical in shape and light-absorbing impurities (LAI), including black carbon, brown carbon, dust, and organics, are assumed to be homogeneously distributed throughout the snow and always external to the ice grain. The

Title Page

Abstract

Introduction

Conclusions

References

Tables

Figures

◀

▶

◀

▶

Back

Close

Full Screen / Esc

Printer-friendly Version

Interactive Discussion



snowpack actinic flux parameterization is used to calculate the UV actinic flux (photons  $\text{cm}^{-2} \text{s}^{-1} \text{nm}^{-1}$ ) and the mean austral summer (DJF) e-folding depths (cm) across Antarctica (Fig. 3a), which are both needed to calculate  $F_{\text{NO}_x}$ . The snowpack actinic flux parameterization is most sensitive to radiation equivalent mean ice grain radii ( $r_e$ ) and insoluble LAI in snow (Zatko et al., 2013); higher concentrations of LAI in the snow and smaller  $r_e$  lead to shallower e-folding depths ( $z_e$ ). It has been recently shown that there are significant increases in surface  $r_e$  throughout austral summer in continental East Antarctica (Dronning Maud Land) (Klein, 2014). The  $r_e$  and snow density values used in this study are from observations reported in Gallet et al. (2011) and Klein (2014) and range from 86–360  $\mu\text{m}$ . The mean Dome C vertical  $r_e$  profile from Gallet et al. (2011) is applied across Antarctica for all seasons except austral summer. During austral summer, larger surface  $r_e$  values are incorporated across all of Antarctica to simulate the rapid surface  $r_e$  growth reported in Klein (2014).

The concentration of black carbon (BC) in the model (Fig. 3b) is calculated by scaling observed BC concentrations ( $C_{\text{BC}}$ ) at Vostok (Grenfell et al., 1994) by the modeled annual average snow accumulation rates ( $\text{kg m}^{-2} \text{year}^{-1}$ ) from GEOS-Chem, which show good agreement with observations (Fig. 2a). However, high accumulation rates in coastal regions ( $700 \text{ kg m}^{-2} \text{year}^{-1}$ ) lead to unrealistically low  $C_{\text{BC}}$ . The minimum  $C_{\text{BC}}$  values used in the model are  $0.08 \text{ ng g}^{-1}$ , which is comparable to the  $C_{\text{BC}}$  values measured in high snow accumulation rate regions in Antarctica, such as in the East Antarctic sea ice zone ( $0.1 \text{ ng g}^{-1}$ ) (Bisiaux et al., 2012; Zatko and Warren, 2015). Insoluble non-black carbon species (nonBC) including dust, brown carbon, and organics, are responsible for the majority (up to 89 % at  $\lambda = 305 \text{ nm}$ ) of the absorption of radiation at UV wavelengths (Zatko et al., 2013) in snow. These nonBC species and their concentrations have not been well quantified in snow. Based on observations reported in Zatko et al. (2013), we scale UV-absorption by insoluble nonBC to the absorption by insoluble black carbon in snow by assuming that insoluble black carbon absorbs 70 % of radiation between  $\lambda = 650\text{--}700 \text{ nm}$ , a wavelength region where black carbon

[Title Page](#)[Abstract](#)[Introduction](#)[Conclusions](#)[References](#)[Tables](#)[Figures](#)[◀](#)[▶](#)[Back](#)[Close](#)[Full Screen / Esc](#)[Printer-friendly Version](#)[Interactive Discussion](#)

dominates absorption, and that nonBC material has an absorption Ångstrom exponent of 5 (Doherty et al., 2010).

We neglect the influence of soluble light absorbers in the snow and only consider the influence of insoluble LAI on calculations of actinic flux profiles in snow. To determine whether soluble LAI contribute significantly to light-absorption in the snow, we calculate the total extinction coefficient for insoluble BC, insoluble nonBC, and soluble LAI following Sect. 2.1 of Zatko et al. (2013) and using the absorption coefficients for soluble material in snow reported in Beine et al., (2011) in northern Alaska. To our knowledge, observations of soluble light-absorbing impurities in Antarctic snow are unavailable. The absorption coefficients ( $0.028 \text{ m}^{-1}$  at  $\lambda = 307 \text{ nm}$ ) from Beine et al. (2011) are identical to the extinction coefficients because it is assumed that there is no scattering by soluble species. Insoluble  $C_{\text{BC}}$  ( $9 \text{ ng g}^{-1}$ ) from Barrow, Alaska (Doherty et al., 2010) were used to calculate extinction coefficients for BC and nonBC material and therefore the amount of nonBC absorption in the UV and near-visible wavelengths following Zatko et al. (2013). Insoluble nonBC material is responsible for 9–14 times more absorption than soluble material in the wavelength range  $\lambda = 298$ – $345 \text{ nm}$ . Insoluble BC material is responsible for 1.5–10 times more absorption than soluble material in the wavelength range  $\lambda = 298$ – $345 \text{ nm}$ . The extinction coefficient is not influenced by the addition of a soluble absorber because scattering by snow grains dominates the extinction in snow. The effective co-albedo of single scattering is increased by 6–15 % when soluble absorbers are included. The resulting change in  $z_e$  is at most 0.5 cm, which represents an increase of 4–9 % in the wavelength region of  $\lambda = 298$ – $345 \text{ nm}$ .

### 2.1.3 Calculating $\text{NO}_3^-$ concentrations in snow

Although there is a large variation in snow  $\text{NO}_3^-$  concentrations from observations collected during the ITASE campaign (Fig. 3d), there is no clear spatial pattern, likely from the redistribution of  $\text{NO}_3^-$  resulting from photolysis and subsequent recycling. The median value of sub-surface snow  $\text{NO}_3^-$  concentration from the ITASE campaign

[Title Page](#)[Abstract](#)[Introduction](#)[Conclusions](#)[References](#)[Tables](#)[Figures](#)[◀](#)[▶](#)[◀](#)[▶](#)[Back](#)[Close](#)[Full Screen / Esc](#)[Printer-friendly Version](#)[Interactive Discussion](#)

( $60 \text{ ng g}^{-1}$ ) (Bertler et al., 2005) is used for sub-surface (below 2 cm) snow  $\text{NO}_3^-$  concentrations ( $[\text{NO}_3^-]_{\text{bot}}$ ) across all of Antarctica in the model. Since  $\text{NO}_3^-$  concentrations in the top 2 cm of snow are up to 10 times higher than  $\text{NO}_3^-$  concentrations below this depth, the  $\text{NO}_3^-$  concentrations in the top 2 cm of snow ( $[\text{NO}_3^-]_{\text{top}}$ ) are calculated by enhancing  $[\text{NO}_3^-]_{\text{bot}}$  by a factor of 6, the median of observed  $\text{NO}_3^-$  enhancement factors (EF) in the top 2 cm of snowpack (Dibb et al., 2004; Frey et al., 2009; Mayewski and Legrand, 1990; Rothlisberger et al., 2000). Since  $\text{NO}_3^-$  concentrations are enhanced by a factor of 6 in the top 2 cm of snow, an equal amount of  $\text{NO}_3^-$  has been removed from the remainder of the photic-zone depth.

As mentioned in the introduction, the measured quantum yields for the dominant  $\text{NO}_3^-$  photolysis pathway (Eq. 1) range from  $1.3 \times 10^{-3} \text{ molec photon}^{-1}$  (Chu and Anastasio, 2003) to  $0.6 \text{ molec photon}^{-1}$  (Zhu et al., 2010). A higher fraction of  $\text{NO}_3^-$  was likely present on ice surfaces in the Zhu et al. (2010) study compared to the Chu and Anastasio (2003) study due to the different sample preparation methods, and likely explains the 3 order-of-magnitude difference in quantum yields. This interpretation suggests  $\text{NO}_3^-$  on the surface of ice grains is much more photolabile compared to  $\text{NO}_3^-$  embedded within ice grains, consistent with results from Meusinger et al. (2014). In this study, we assume that  $\text{NO}_3^-$  that is wet deposited to the snow surface is more likely to be embedded in the interior of a snow grain compared to  $\text{NO}_3^-$  that is dry deposited to the surface of the snow grain. To account for this effect, we scale snow  $\text{NO}_3^-$  concentrations by the fraction of dry deposition relative to total (wet + dry) deposition to the Antarctic snow surface (Fig. 3c), assuming that only the fraction of dry deposited  $\text{NO}_3^-$  is photolabile ( $F_p$ ). The degree of migration of  $\text{NO}_3^-$  within a snow grain after deposition due to snow metamorphism is unknown, which may influence the photolability of  $\text{NO}_3^-$  (Domine and Shepson, 2002). Snow  $\text{NO}_3^-$  concentrations scaled by  $F_p$  are shown in Fig. 3d.

Other modeling studies have attempted to calculate the fraction of photolabile  $\text{NO}_3^-$  in snow by estimating the concentration of  $\text{NO}_3^-$  contained within the liquid-like region

[Title Page](#)[Abstract](#)[Introduction](#)[Conclusions](#)[References](#)[Tables](#)[Figures](#)[◀](#)[▶](#)[◀](#)[▶](#)[Back](#)[Close](#)[Full Screen / Esc](#)[Printer-friendly Version](#)[Interactive Discussion](#)

(LLR) on the surface of ice grains (e.g., Thomas et al., 2012). In this work, we do not explicitly calculate  $\text{NO}_3^-$  photolysis within the LLR because there are still many unknowns about the LLR (Domine et al., 2013), including the distribution of  $\text{NO}_3^-$  between the bulk snow and the LLR. This distribution is better understood for some species, such as chloride (Cho et al., 2002), but it is unclear if  $\text{NO}_3^-$  behaves similarly. The quantum yield for  $\text{NO}_3^-$  photolysis is dependent on the location of  $\text{NO}_3^-$  in snow, and although there are uncertainties surrounding the location of  $\text{NO}_3^-$  in snow, in this study we use the full range of measured quantum yields to provide bounds for the amount of  $\text{NO}_x$  produced from snow  $\text{NO}_3^-$  photolysis.

## 10 2.2 Model sensitivity studies

Due to uncertainties in our understanding of snow photochemistry (Domine et al., 2013), we perform a variety of model sensitivity studies, as shown in Table 2. The quantum yield is varied from  $1.3 \times 10^{-3}$  molec photon $^{-1}$  (Chu and Anastasio, 2003) to 0.6 molec photon $^{-1}$  (Zhu et al., 2010). Snow  $\text{NO}_3^-$  concentrations below 2 cm ( $[\text{NO}_3^-]_{\text{bot}}$ ) are halved and doubled with respect to the base case scenario and the impact of scaling  $\text{NO}_3^-$  concentrations by the fraction of photolabile  $\text{NO}_3^- (F_p)$  is investigated. The  $\text{NO}_3^-$  enhancement factor in the top 2 cm of snowpack is varied from 1 to 10, based upon a range of reported observations (Dibb et al., 2004; Frey et al., 2009; Mayewski and Legrand, 1990; Rothlisberger et al., 2000).  $C_{\text{BC}}$  is halved and doubled with respect to the base case scenario. The  $r_e$  profiles are varied in three sensitivity studies to examine the influence of  $r_e$  on the model-calculated mean austral summer (DJF) flux of snow-sourced  $\text{NO}_x$  ( $\overline{F}_{\text{NO}_x}$ ). The bulk extinction coefficient for snow ( $K_{\text{ext,tot}}$ ) is increased and decreased by 20 % with respect to the base case scenario because Libois et al. (2013) suggest that the spherical snow grain assumption overestimates e-folding depths by a factor of 1.2. These sensitivity studies are used to provide estimates of the influence of these parameters on  $\overline{F}_{\text{NO}_x}$  throughout the Antarctic continent.



## 2.3 Estimating the impact of snow $\text{NO}_3^-$ photolysis on boundary layer chemistry and ice-core $\text{NO}_3^-$ records

ACPD

15, 18963–19015, 2015

### The impact of snow nitrate photolysis in Antarctica

M. C. Zatko et al.

Nitrate photolysis followed by oxidation, recycling, and redistribution of snow-sourced  $\text{NO}_x$  influences both boundary layer chemistry and the preservation of  $\text{NO}_3^-$  in ice-core records. The preservation of  $\text{NO}_3^-$  in ice cores is most dependent on the amount of  $\text{NO}_3^-$  lost from the snow through photolysis via transport of snow-sourced  $\text{NO}_x$  away from the site of primary deposition. The methods used to explore and quantify nitrogen recycling and photolysis-driven loss of  $\text{NO}_3^-$  in snow are described in the following sections.

#### 2.3.1 Reactive nitrogen recycling between the air and snow

- 10 The Nitrogen Recycling Factor ( $\text{NRF}_{\text{year}}$ ) is a metric proposed by Davis et al. (2008) to quantify the degree of reactive nitrogen recycling in snow over 1 year.

$$\text{NRF}_{\text{year}} = \frac{F_{\text{NO}_x}}{F_{\text{PRI}}} . \quad (8)$$

In Eq. (8),  $F_{\text{NO}_x}$  ( $\text{ng N m}^{-2} \text{year}^{-1}$ ) is the annual sum of  $\text{NO}_x$  released from the snow and  $F_{\text{PRI}}$  ( $\text{ng N m}^{-2} \text{year}^{-1}$ ) is the annual sum of primary  $\text{NO}_3^-$  deposited to the snow.

- 15 Davis et al. (2008) use the  $\text{NRF}_{\text{year}}$  to describe nitrogen recycling on both macro-scale (e.g., across the East Antarctic plateau) and micro-scale (e.g., the number of times one molecule of  $\text{NO}_3^-$  is recycled) levels. An  $\text{NRF}_{\text{year}}$  greater than 1 suggests that multiple nitrogen recycling events occur in the snow. The  $\text{NRF}_{\text{year}}$  has implications for boundary layer chemistry because the continual re-emission of  $\text{NO}_x$  enhances the effective concentration of  $\text{NO}_x$  in the boundary layer (Davis et al., 2008).

We calculate the number of years that  $\text{NO}_3^-$  remains in the photic zone ( $\tau_z$ , years) according to Eq. (9), where both the depth of the photic zone (cm) and the total annual

<a href="#">Title Page</a>	<a href="#">Abstract</a>	<a href="#">Introduction</a>
<a href="#">Conclusions</a>	<a href="#">References</a>	
<a href="#">Tables</a>	<a href="#">Figures</a>	
<a href="#">◀</a>	<a href="#">▶</a>	
<a href="#">◀</a>	<a href="#">▶</a>	
<a href="#">Back</a>	<a href="#">Close</a>	
<a href="#">Full Screen / Esc</a>		
	<a href="#">Printer-friendly Version</a>	
	<a href="#">Interactive Discussion</a>	



snow accumulation ( $\alpha_r$ , cm year $^{-1}$ ) are considered.

$$\tau_z = \frac{z_e}{\alpha_r}, \quad (9)$$

where  $z_e$  (cm) is 1 e-folding depth. For Eqs. (9)–(12) we use  $z_e$  instead of  $z_{3e}$  because 87–91 % of snow-sourced  $\text{NO}_x$  is produced within the top 1 e-folding depth ( $z_e$ ). To convert total annual snow accumulation rate (Fig. 2a) from  $\text{kg m}^{-2} \text{year}^{-1}$  to cm, a typical snow density for Antarctica ( $0.36 \text{ g cm}^{-3}$ ) (Grenfell et al., 1994) is assumed.  $\tau_z$  is the minimum number of years on average that  $\text{NO}_3^-$  remains in the top one-third of the snow photic zone before burial beneath because nitrogen recycling, which effectively redistributes  $\text{NO}_3^-$  upwards in the snow, is not factored into Eq. (9).  $\tau_z$  thus represents the lifetime of  $\text{NO}_3^-$  in snow in an average sense and does not resolve photolysis and recycling of individual  $\text{NO}_3^-$  molecules.

The degree of recycling of  $\text{NO}_3^-$  in ice-core records is dependent on the total number of times that  $\text{NO}_3^-$  is recycled between the air and snow before burial beneath the photic zone. We assume no further photolysis or recycling of  $\text{NO}_3^-$  below the photic zone. In many locations in Antarctica,  $\text{NO}_3^-$  is recycled between the air and snow for multiple years before burial (Sect. 3.3). To calculate the total degree of recycling between the time of primary  $\text{NO}_3^-$  deposition and burial beneath the photic zone, the  $\text{NRF}_{\text{year}}$  in Eq. (9) is multiplied by  $\tau_z$  ( $\text{NRF}_{\tau_z}$ ) as shown in Eq. (10).

$$\text{NRF}_{\tau_z} = \frac{F_{\text{NO}_x}}{F_{\text{PRI}}} \cdot \tau_z. \quad (10)$$

Similar to the  $\text{NRF}_{\text{year}}$  in Eq. (9),  $\text{NRF}_{\tau_z}$  values greater than 1 suggests that multiple nitrogen recycling events are occurring in the snow before burial beneath the photic zone.  $\text{NRF}_{\tau_z}$  represents the average, or “bulk” degree of nitrogen recycling in snow before  $\text{NO}_3^-$  is ultimately preserved in ice cores. This global modeling study cannot resolve the degree of nitrogen recycling on a molecular level in the snow; some  $\text{NO}_3^-$

[Title Page](#)

[Abstract](#)

[Introduction](#)

[Conclusions](#)

[References](#)

[Tables](#)

[Figures](#)

◀

▶

◀

▶

[Back](#)

[Close](#)

[Full Screen / Esc](#)

[Printer-friendly Version](#)

[Interactive Discussion](#)



molecules may never be photolyzed while other  $\text{NO}_3^-$  molecules may be photolyzed and recycled many times greater than  $\text{NRF}_{\tau_z}$ .

### 2.3.2 Export of nitrate away from the original site of photolysis

Once snow-sourced  $\text{NO}_x$  is emitted to the atmosphere, it is subject to transport away from the original site of photolysis. If snow-sourced  $\text{NO}_x$  is oxidized to  $\text{HNO}_3$  and redeposited back to the snow surface, then there is no net photolysis-driven loss of  $\text{NO}_3^-$  from the snow. However, if some of the snow-sourced  $\text{NO}_x$  is transported away from the site of primary deposition, there is a net photolysis-driven loss of  $\text{NO}_3^-$  from the snow.

The fraction of total  $\text{NO}_3^-$  (photolabile + non-photolabile) lost from the snow driven by photolysis ( $f$ ) is calculated in Eq. (11):

$$f = \left( 1 - \left( \frac{F_R}{F_{\text{NO}_x}} \right)^{\tau_z} \right) \cdot F_p . \quad (11)$$

In Eq. (11),  $F_R$  ( $\text{ng N m}^{-2} \text{year}^{-1}$ ) is the total annual flux of recycled  $\text{NO}_3^-$  to the snow surface and  $F_{\text{NO}_x}$  ( $\text{ng N m}^{-2} \text{year}^{-1}$ ) is the total annual flux of  $\text{NO}_x$  released from the snow.  $F_R$  is calculated by subtracting the depositional flux of  $\text{NO}_3^-$  from a model run without snow photochemistry from the depositional flux of  $\text{NO}_3^-$  from a model run with snow photochemistry. The ratio of  $F_R$  to  $F_{\text{NO}_x}$  represents the fraction of photolabile  $\text{NO}_3^-$  remaining in the snow after 1 year. As long as  $\text{NO}_3^-$  remains in the photic zone,  $\text{NO}_3^-$  can continually be photolyzed and recycled. The preservation of  $\text{NO}_3^-$  in ice cores is dependent on the fraction of  $\text{NO}_3^-$  lost from the snow through photolysis during the entire time that  $\text{NO}_3^-$  remains in the photic zone. Provided that there are not major changes in parameters that influence snow photochemistry (e.g., LAI, overhead ozone abundance) from year to year, the fraction of photolabile  $\text{NO}_3^-$  lost from the snow will be stable from year to year.  $\tau_z$  in Eq. (11) accounts for the loss of  $\text{NO}_3^-$  that occurs during the entire time that it remains in the photic zone. When  $\text{NO}_3^-$  remains in the photic zone for less

<a href="#">Title Page</a>	
<a href="#">Abstract</a>	<a href="#">Introduction</a>
<a href="#">Conclusions</a>	<a href="#">References</a>
<a href="#">Tables</a>	<a href="#">Figures</a>
<a href="#">◀</a>	<a href="#">▶</a>
<a href="#">◀</a>	<a href="#">▶</a>
<a href="#">Back</a>	<a href="#">Close</a>
<a href="#">Full Screen / Esc</a>	
<a href="#">Printer-friendly Version</a>	
<a href="#">Interactive Discussion</a>	



## The impact of snow nitrate photolysis in Antarctica

M. C. Zatko et al.

[Title Page](#)

[Abstract](#)

[Introduction](#)

[Conclusions](#)

[References](#)

[Tables](#)

[Figures](#)

[◀](#)

[▶](#)

[◀](#)

[▶](#)

[Back](#)

[Close](#)

[Full Screen / Esc](#)

[Printer-friendly Version](#)

[Interactive Discussion](#)



- than a year ( $\tau_z < 1$ ),  $\tau_z$  in Eq. (11) is set equal to 1. In Eq. (11),  $\left(1 - \left(F_R/F_{NO_x}\right)^{\tau_z}\right)$  represents the fraction of photolabile  $NO_3^-$  lost from the snow through photolysis. This fraction is multiplied by  $F_p$  to calculate the fraction of total (photolabile + non-photolabile)  $NO_3^-$  lost from the snow through photolysis ( $f$ ). If  $f$  is 0, then all snow-sourced  $NO_x$  is redeposited to the snow and there is no net loss of  $NO_3^-$ .  $f$  is also 0 if the net export of snow-sourced  $NO_x$  away from the site of original photolysis is balanced by net import of snow-sourced  $NO_x$  from other Antarctic locations. If  $f$  is between 0 and 1, the export of local snow-sourced  $NO_x$  is higher than the deposition of snow-sourced  $NO_x$  from elsewhere in Antarctica, resulting in net photolysis-driven loss of  $NO_3^-$  from the snow. If  $f$  is less than 0, the export of local snow-sourced  $NO_x$  is lower than the deposition of snow-sourced  $NO_x$  from elsewhere in Antarctica, resulting in net photolysis-driven gain of  $NO_3^-$  to the snow.

$f$  is used to calculate the enrichment in ice-core  $\delta^{15}N(NO_3^-)$  due solely to the impact of photolysis-driven loss of  $NO_3^-$  in snow. We use a Rayleigh fractionation equation used to calculate  $\delta^{15}N(NO_3^-)$  (Blunier et al., 2005):

$$\delta^{15}N(NO_3^-) = \delta^{15}N(NO_3^-)_{air} \cdot (1 - f)^\varepsilon - 1. \quad (12)$$

In Eq. (12),  $\delta^{15}N(NO_3^-)_{air}$  is the annual-averaged  $\delta^{15}N$  value of boundary layer  $NO_3^-$  and  $\varepsilon$  is the fractionation constant (-47.9‰, Berhanu et al., 2014). In this work, we set  $\delta^{15}N(NO_3^-)_{air}$  equal to 0‰ to investigate the enrichment in  $\delta^{15}N(NO_3^-)$  only from photolysis-driven loss of  $NO_3^-$  from snow.

### 3 Results and discussion

#### 3.1 Parameters that influence $F_{\text{NO}_x}$ and its spatial redistribution

Figure 2a shows modeled total annual snow accumulation rates from GEOS-Chem ( $\text{kg m}^{-2} \text{year}^{-1}$ ) along with estimated total annual snow accumulation rates ( $\text{kg m}^{-2} \text{year}^{-1}$ ) in Antarctica (Erbland et al., 2013; Grenfell et al., 1994; Sofen et al., 2014), ranging from  $10\text{--}700 \text{kg m}^{-2} \text{year}^{-1}$ . The rapid decrease in snow accumulation rate from the coast to the top of the East Antarctic plateau is attributed to increased distance from the ocean (moisture source) and increased elevation. There is good agreement between the modeled total snow accumulation rates in GEOS-Chem and previously reported total annual snow accumulation rates. Figure 2b shows modeled annual mean surface wind divergence from May 2009 to May 2010; which is in general agreement with Antarctic Mesoscale Prediction System surface wind output from Fig. 3 in Parish and Bromwich (2007). The annual mean surface wind patterns indicate that the large-scale airflow pattern in Antarctica flows from the East Antarctic plateau downslope towards the coast. There are three major regions of wind convergence in Antarctica, located near the Ross, Ronne, and Amery ice shelves.

Figure 3a shows the mean austral summer (DJF) e-folding depth of UV actinic flux in snow ( $z_e$ ).  $z_e$  ranges from 24 to 69 cm, with the shallowest depths on the East Antarctic plateau, due to the relatively high  $C_{\text{BC}}$  values (Fig. 3b). Higher  $C_{\text{BC}}$  in snow results in a shallower  $z_e$  because UV absorption in snow is enhanced as the concentration of LAI increases (Zatko et al., 2013). In this study, coastal grid boxes are a mixture of water, sea ice, and snow-covered surfaces, and since actinic flux profiles are only calculated for snow-covered surfaces, the average  $z_e$  in coastal grid boxes are artificially shallow. Observations of e-folding depths across Antarctica are limited. France et al. (2011) report  $z_e$  from near-station snow at Dome C ranging from 9–20 cm at 350 nm, which agree well with our modeled  $z_e$  (Zatko et al., 2013). There are no  $z_e$  observations in Antarctica from snow without station contamination, which is representative of the majority of snow in Antarctica. Zatko et al. (2013) calculate  $z_e$  of 38 cm ( $\lambda = 298\text{--}345 \text{nm}$ )

<a href="#">Title Page</a>	
<a href="#">Abstract</a>	<a href="#">Introduction</a>
<a href="#">Conclusions</a>	<a href="#">References</a>
<a href="#">Tables</a>	<a href="#">Figures</a>
<a href="#"></a>	<a href="#"></a>
<a href="#"></a>	<a href="#"></a>
<a href="#">Full Screen / Esc</a>	
<a href="#">Printer-friendly Version</a>	
<a href="#">Interactive Discussion</a>	



<a href="#">Title Page</a>	
<a href="#">Abstract</a>	<a href="#">Introduction</a>
<a href="#">Conclusions</a>	<a href="#">References</a>
<a href="#">Tables</a>	<a href="#">Figures</a>
<a href="#">◀</a>	<a href="#">▶</a>
<a href="#">◀</a>	<a href="#">▶</a>
<a href="#">Back</a>	<a href="#">Close</a>
<a href="#">Full Screen / Esc</a>	
<a href="#">Printer-friendly Version</a>	
<a href="#">Interactive Discussion</a>	

for remote Dome C snow due to lower  $C_{BC}$  far away from station contamination. The  $z_e$  for remote Dome C snow in this study (48 cm) is a factor of 1.3 larger than reported in Zatko et al. (2013) because larger radiation equivalent ice grain radii ( $r_e$ ) are used during austral summer (based on Klein (2014)), and larger  $r_e$  grains lead to deeper  $z_e$ .

Figure 3b shows snow  $C_{BC}$ , ranging from 0.08 to 0.6 ng g<sup>-1</sup>. Black carbon observations at WAIS-Divide (Bisiaux et al. 2012), Byrd (Chylek et al., 1992), Vostok (Grenfell et al., 1994), South Pole (Warren and Clarke, 1990), and Dome C (Warren et al., 2006) are included in Fig. 3b. There is good agreement between the modeled and observed  $C_{BC}$ . The highest  $C_{BC}$  values in Antarctica are found on the East Antarctic plateau (0.6 ng g<sup>-1</sup>) and the spatial pattern of  $C_{BC}$  is governed by the snow accumulation rate; higher snow accumulation rates dilute  $C_{BC}$  (Doherty et al., 2013). The modeled boundary layer black carbon concentrations are relatively uniform across Antarctica (0.1–0.6 pptv) because the majority of black carbon reaches Antarctica through long-range transport (with the exception of local production from Antarctic research stations).

Figure 3c shows the fraction of dry-deposited  $\text{NO}_3^-$  compared to total deposited  $\text{NO}_3^-$  across Antarctica. The ratio of dry deposition to total deposition ranges from 0 to 0.2 in coastal Antarctica and from 0.95 to 0.99 on the East Antarctic plateau. Figure 3d shows the modeled annual average sub-surface (below 2 cm) snow  $\text{NO}_3^-$  concentrations (60 ng g<sup>-1</sup>) scaled by  $F_p$  compared to averaged multi-year  $\text{NO}_3^-$  observations from the ITASE campaign (3.7–797 ppb) (Bertler et al., 2005).

### 3.2 Model sensitivity studies

Table 2 shows the dependence of mean austral summer (DJF)  $\overline{F_{\text{NO}_x}}$  on  $\phi$ ,  $[\text{NO}_3^-]_{\text{bot}}$ ,  $C_{BC}$ ,  $F_p$ ,  $K_{\text{ext,tot}}$ ,  $r_e$ . The sensitivity study results are compared to  $\overline{F_{\text{NO}_x}}$  from the base case scenario, which is also described in Table 2.  $\overline{F_{\text{NO}_x}}$  is most sensitive to  $\phi$ , which increases  $\overline{F_{\text{NO}_x}}$  by up to a factor of 400 compared to the base case scenario. The second most influential parameter is the concentration of photolabile  $\text{NO}_3^-$  ( $[\text{NO}_3^-]_{\text{bot}}$ )



and  $F_p$ ), which changes  $\overline{F_{NO_x}}$  by up to a factor of 7.4 (at the coasts) with respect to the base case scenario. Variations in  $r_e$ ,  $K_{ext,tot}$ , EF, and  $C_{BC}$  influence  $\overline{F_{NO_x}}$  by up to a factor of 1.3 compared to the base case scenario.

Figure 4 shows model-calculated mean austral summer (DJF)  $\overline{F_{NO_x}}$  for several sensitivity studies compared to previously reported  $\overline{F_{NO_x}}$  at Neumayer (Jones et al., 2001), Halley (Bauguitte et al., 2012; Jones et al., 2011), South Pole (Oncley et al., 2004; Wang et al., 2008; Zatko et al., 2013), Dome C (Frey et al., 2013; Zatko et al., 2013), and WAIS-Divide (Mascllin et al., 2013). The flux of snow-sourced  $NO_x$  is overestimated by three orders of magnitude compared to observations when  $\phi$  from Zhu et al. (2010) is used to calculate  $\overline{F_{NO_x}}$ . In contrast, model-calculated  $\overline{F_{NO_x}}$  using  $\phi$  from Chu and Anastasio (2003) provides better agreement with the observations, but underestimates the observations by 14–78 %. Use of the fraction of dry-deposited  $NO_3^-$  to scale the concentration of photolabile  $NO_3^-$  ( $F_p$ ) lowers  $\overline{F_{NO_x}}$  by up to 85 % along the coast, but has little impact on the East Antarctic plateau due to the high fraction of dry deposited  $NO_3^-$  (Fig. 3c). The spatial patterns of  $\overline{F_{NO_x}}$  in Fig. 4 are largely governed by the depth of the photic zone ( $z_e$ ) across Antarctica (Fig. 3a), which are inversely related to LAI concentrations. The spatial patterns of  $\overline{F_{NO_x}}$  are also influenced by the fraction of photolabile  $NO_3^-$ , which is lowest at the coast in the model.

Observations of  $F_{NO_x}$  are calculated from measurements of  $NO_x$  concentration gradients and turbulent diffusivity (Jones et al., 2001, 2011; Frey et al., 2013) or calculated based on observed NO gradients and assuming photochemical steady-state (Oncley et al., 2004), by incorporating observations into 1-D chemistry models (Bauguitte et al., 2012; Wang et al., 2008), or by using depth-integrated  $F_{NO_x}$  calculations similar to Eq. (7) (Mascllin et al., 2013; Zatko et al., 2013). Observations of  $F_{NO_x}$  represent either noontime maxima (Bauguitte et al., 2012; Frey et al., 2013; Jones et al., 2001; Zatko et al., 2013), daily averages (Jones et al., 2011; Mascllin et al., 2013), or averages over the duration of the field campaign (Oncley et al., 2004; Wang et al., 2008) (see Table 4 in Mascllin et al., 2013). Regardless of the time period that the  $F_{NO_x}$  observations rep-

[Title Page](#)[Abstract](#)[Introduction](#)[Conclusions](#)[References](#)[Tables](#)[Figures](#)[◀](#)[▶](#)[◀](#)[▶](#)[Back](#)[Close](#)[Full Screen / Esc](#)[Printer-friendly Version](#)[Interactive Discussion](#)

resent, all  $F_{NO_x}$  values for each location are averaged together and presented in Fig. 4c and d. There is a wide range of reported  $\overline{F_{NO_x}}$  at many of these locations (Mascllin et al., 2013) and comparing the mean  $\overline{F_{NO_x}}$  observation at each site with modeled  $\overline{F_{NO_x}}$  values in this study allows for a coarse examination of the model-measurement agreement. 5 Unfortunately, the actinic flux parameterization used here (Zatko et al., 2013) is unable to resolve  $\overline{F_{NO_x}}$  directly at the coast because coastal grid boxes are a mixture of ocean, sea ice, and land, which prevents direct comparison of  $\overline{F_{NO_x}}$  at Halley and Neumayer. The modeled  $\overline{F_{NO_x}}$  shown in Fig. 4c and d are in rough agreement with observations (order of magnitude) at Dome C, South Pole, and WAIS-Divide, although modeled  $\overline{F_{NO_x}}$  10 values are lower than observations, regardless of whether  $NO_3^-$  is scaled by  $F_p$ . Since the flux of snow-sourced  $NO_x$  is overestimated by three orders of magnitude compared to observations when the quantum yield from Zhu et al. (2010) is used, all following results (Figs. 5–11) are calculated using the Chu and Anastasio (2003) quantum yield ( $\phi = 1.3 \times 10^{-3}$  molec photon $^{-1}$ ). Additionally, to approximate the potential spatial variability in the fraction of  $NO_3^-$  that is photolabile, we scale snow  $NO_3^-$  by  $F_p$  in Figs. 5–11. 15 Figure 4d shows the  $\overline{F_{NO_x}}$  values, ranging from  $0.5\text{--}7.8 \times 10^8$  molec cm $^{-2}$  s $^{-1}$ , used in Figs. 5–11. All the other parameters used to calculate  $\overline{F_{NO_x}}$  in following sections and in Figs. 5–11 are described in the base-case scenario in Table 2.

### 3.3 Redistribution and recycling of reactive nitrogen across Antarctica

20 Figure 5a shows the total annual depositional flux of primary  $NO_3^-$  ( $F_{PRI}$ ), which ranges from  $0.9\text{--}35 \times 10^5$  ng N m $^{-2}$  year $^{-1}$  and is highest at the coasts due to its relative proximity to  $NO_x$ -source regions in lower latitudes. An adjoint modeling study by Lee et al. (2014) suggests that boundary layer  $NO_3^-$  abundance in Antarctica is dominated by  $NO_3^-$  transport to Antarctica originating from  $NO_x$  emissions from 25–65° S during austral winter and by thermal decomposition of peroxyacetyl nitrates (PAN) as it descends

<a href="#">Title Page</a>	
<a href="#">Abstract</a>	<a href="#">Introduction</a>
<a href="#">Conclusions</a>	<a href="#">References</a>
<a href="#">Tables</a>	<a href="#">Figures</a>
<a href="#">◀</a>	<a href="#">▶</a>
<a href="#">◀</a>	<a href="#">▶</a>
<a href="#">Back</a>	<a href="#">Close</a>
<a href="#">Full Screen / Esc</a>	
<a href="#">Printer-friendly Version</a>	
<a href="#">Interactive Discussion</a>	



from the free troposphere in all other seasons. Figure 5b shows the total annual depositional flux of recycled  $\text{NO}_3^-$  ( $F_R$ ), which ranges from  $0.7\text{--}31 \times 10^5 \text{ ng N m}^{-2} \text{ year}^{-1}$  and is also highest at the coasts due to transport from the Antarctic interior by katabatic winds.  $F_{\text{PRI}}$  and  $F_R$  are comparable in magnitude to the total annual flux of snow-sourced  $\text{NO}_x$  to the atmosphere ( $F_{\text{NO}_x}$ ), which ranges from  $2\text{--}23 \times 10^5 \text{ ng N m}^{-2} \text{ year}^{-1}$  (Fig. 4d). Figure 5c shows recycled nitrogen ( $F_R$ ) is the dominant form of  $\text{NO}_3^-$  deposition across Antarctica, except along the coastline where it represents as little as 11% of the deposition flux, and is most important in regions of wind convergence such as the Ronne, Ross, and Amery ice shelves.

To further investigate the role that wind patterns have on the redistribution of  $\text{NO}_3^-$  across Antarctica, we alternately turn off the upward  $F_{\text{NO}_x}$  in East Antarctica and in West Antarctica to examine the influence of each region on  $\text{NO}_3^-$  redistribution across Antarctica. Figure 6 compares  $F_R$  in these sensitivity studies to  $F_R$  in the base case scenario. The large reduction in  $F_R$  when  $F_{\text{NO}_x}$  is separately turned off in East and West Antarctica demonstrates that little snow-sourced  $\text{NO}_3^-$  is transported between East and West Antarctica, likely due to the influence of the trans-Antarctic mountains on atmospheric transport. However, recycled  $\text{NO}_3^-$  is present in West Antarctica where  $F_{\text{NO}_x}$  has been turned off, suggesting that some snow-sourced  $\text{NO}_3^-$  from East Antarctica is transported across the trans-Antarctic mountains likely due to the influence of katabatic winds originating from the East Antarctic plateau.

Figure 7a shows the Nitrogen Recycling Factor ( $\text{NRF}_{\text{year}}$ ). Across Antarctica,  $\text{NRF}_{\text{year}}$  ranges from 0 to 16, indicating that nitrogen is recycled multiple times over the course of 1 year across most of Antarctica, with the exception of the coasts. The spatial pattern of  $\text{NRF}_{\text{year}}$  is governed by the flux of snow-sourced  $\text{NO}_x$  to the atmosphere ( $\overline{F}_{\text{NO}_x}$ , Fig. 4d), which is influenced by the depth of the photic zone ( $z_e$ ) and the concentration of photolabile nitrate.  $\text{NRF}_{\text{year}}$  values are lowest near the coast because the fraction of photolabile  $\text{NO}_3^-$  is small and  $F_{\text{PRI}}$  values are high. The maximum  $\text{NRF}_{\text{year}}$  values occur partway up the plateau, corresponding to maximum  $\overline{F}_{\text{NO}_x}$  values. (Fig. 4d). The

M. C. Zatko et al.

[Title Page](#)

[Abstract](#)

[Introduction](#)

[Conclusions](#)

[References](#)

[Tables](#)

[Figures](#)

◀

▶

◀

▶

[Back](#)

[Close](#)

[Full Screen / Esc](#)

[Printer-friendly Version](#)

[Interactive Discussion](#)



East Antarctic  $\text{NRF}_{\text{year}}$  value (1.8) calculated in Davis et al. (2008) is over 3 times lower than the East Antarctic  $\text{NRF}_{\text{year}}$  values shown in Fig. 7a. The disagreement in  $\text{NRF}_{\text{year}}$  values is likely due to the varying approaches used to estimate  $F_{\text{NO}_x}$  and  $F_{\text{PRI}}$  in each study.

- Figure 7b shows the minimum number of years that snow  $\text{NO}_3^-$  remains in the photic zone on average,  $\tau_z$  (Eq. 9). Nitrate remains in photic zone for 3 months near the Antarctic coasts and up to 7.5 years on the East Antarctic plateau before burial. The spatial pattern of  $\tau_z$  is governed by the snow accumulation rate, both directly and indirectly through its influence on  $C_{\text{BC}}$ . The spatial pattern of  $\tau_z$  is in agreement with the expectation that  $\text{NO}_3^-$  remains in the photic zone the longest in areas with low snow accumulation rates.

- Figure 7c shows  $\text{NRF}_{\tau_z}$  (Eq. 10) across Antarctica, which is an estimate of the number of times that  $\text{NO}_3^-$  is recycled before burial beneath the photic zone.  $\text{NRF}_{\tau_z}$  ranges from 0 to 57, and is highest on the East Antarctic plateau. Similar to  $\text{NRF}_{\text{year}}$ , the lowest  $\text{NRF}_{\tau_z}$  values are near the coasts. Unlike the  $\text{NRF}_{\text{year}}$ , the highest  $\text{NRF}_{\tau_z}$  values are on the East Antarctic plateau, where  $\tau_z$  values are highest.  $\text{NRF}_{\tau_z}$  varies by over two orders of magnitude between the Antarctic coast and the interior plateau, which suggests that the degree of  $\text{NO}_3^-$  preservation in ice cores varies dramatically across Antarctica. Erbland et al. (2015) use a multi-layer snow chemistry column model to estimate the number of times  $\text{NO}_3^-$  is recycled before burial ( $\text{NRF}_{\tau_z}$ ) at Dome C and have very recently estimated that  $\text{NO}_3^-$  is recycled 4 times before burial below the photic zone at Dome C. The  $\text{NRF}_{\tau_z}$  value calculated in Erbland et al. (2015) is more similar in magnitude to the Dome C  $\text{NRF}_{\text{year}}$  value (9) calculated in this study compared to  $\text{NRF}_{\tau_z}$  value (53). The disagreement in  $\text{NRF}_{\tau_z}$  values is currently being investigated, but these two modeling studies likely provide upper and lower limits for the number of times that  $\text{NO}_3^-$  is recycled before burial below the snow photic zone at Dome C.

<a href="#">Title Page</a>	
<a href="#">Abstract</a>	<a href="#">Introduction</a>
<a href="#">Conclusions</a>	<a href="#">References</a>
<a href="#">Tables</a>	<a href="#">Figures</a>
<a href="#">◀</a>	<a href="#">▶</a>
<a href="#">◀</a>	<a href="#">▶</a>
<a href="#">Back</a>	<a href="#">Close</a>
<a href="#">Full Screen / Esc</a>	
<a href="#">Printer-friendly Version</a>	
<a href="#">Interactive Discussion</a>	



### 3.4 Impact of reactive nitrogen recycling on boundary layer chemistry

The height of the boundary layer will strongly influence the abundance of  $\text{NO}_3^-$ , reactive nitrogen oxides, and oxidants emitted or formed at or near the surface. At many Antarctic stations (e.g., Neumayer, South Pole, Dome C, Halley, Kohnen) there is a wide range of observed boundary layer heights during austral summer (10–600 m; Casasanta et al., 2014; Davis et al., 2004; Handorf, 1996; Jones et al., 2006, 2008; King et al., 2006; Kodama et al., 1985; Konig-Langlo et al., 1998; Neff et al., 2008; Oncley et al., 2004; Travouillon et al., 2008; Weller et al., 1999), and although modeled boundary layer heights are not systematically biased in one direction compared to observations, they often do not agree well. Therefore, only the relative impacts of snow photochemistry on reactive nitrogen and oxidant abundances are compared in this study. The impact of snow photochemistry on boundary layer chemistry can be examined by considering factor changes in boundary layer  $\text{NO}_x$ ,  $\text{NO}_3^-$ , OH, and  $\text{O}_3$  mixing ratios between simulations with and without snow  $\text{NO}_3^-$  photolysis. As shown in Fig. 8, the inclusion of a snow  $\text{NO}_x$  source leads to factor increases in boundary layer mixing ratios of  $\text{NO}_x$  from 7.0–31.6, gas-plus aerosol-phase nitrate from 3.9–38.1, OH from 3.6–6.7, and  $\text{O}_3$  from 1.3–2.0. The largest factor increases are in West Antarctica, particularly near the Ross and Ronne ice shelves, where winds carrying photo-produced species converge. The surface transport pattern is especially important for the redistribution of the longer-lived species  $\text{NO}_3^-$  and  $\text{O}_3$ . Other snow photochemical reactions mentioned in the introduction but not included in this modeling study will also impact oxidant abundances, but the effects of each photochemical reaction will not be additive due to the highly non-linear nature of oxidant cycling.

### 3.5 Implications for ice-core records of $\text{NO}_3^-$ concentrations and isotopes

Figure 9a shows the fraction of  $\text{NO}_3^-$  lost from the snow through photolysis ( $f$ , Eq. 11), which ranges from –0.21 to 0.99. The negative  $f$  values indicate regions with net gain of  $\text{NO}_3^-$  to the snow resulting from the spatial redistribution of  $\text{NO}_3^-$  driven by snow

[Title Page](#)[Abstract](#)[Introduction](#)[Conclusions](#)[References](#)[Tables](#)[Figures](#)[◀](#)[▶](#)[◀](#)[▶](#)[Back](#)[Close](#)[Full Screen / Esc](#)[Printer-friendly Version](#)[Interactive Discussion](#)

**The impact of snow nitrate photolysis in Antarctica**

M. C. Zatko et al.

photochemistry. In regions of convergence, such as over the Ronne Ice Shelf, and parts of the coast, there is a net gain of snow-sourced  $\text{NO}_3^-$ . There is a sharp gradient in  $f$  between the plateau and the coast, with the largest loss of snow  $\text{NO}_3^-$  on the East Antarctic plateau. On the East Antarctic plateau, most photolyzed  $\text{NO}_3^-$  is transported away by katabatic winds, but along the coast, the photolysis-driven loss of  $\text{NO}_3^-$  from the snow is minimal due to high snow accumulation rates and transport of snow-sourced  $\text{NO}_3^-$  from the continental interior. The spatial pattern of  $f$  is largely influenced by the number of years that  $\text{NO}_3^-$  remains in the photolytic zone ( $\tau_z$ ), the concentration of photolabile  $\text{NO}_3^-$  ( $F_p$ ), and wind patterns across Antarctica.

Figure 9b shows modeled enrichments in ice-core  $\delta^{15}\text{N}(\text{NO}_3^-)$  from photolysis-driven loss of  $\text{NO}_3^-$  in snow compared to sub-photic zone  $\delta^{15}\text{N}(\text{NO}_3^-)$  observations from Erbland et al. (2013), Frey et al. (2009), Jarvis (2008), Shi et al. (2014), and Sofen et al. (2014). The  $\delta^{15}\text{N}(\text{NO}_3^-)$  values at Dome C and along the transect from Dumont D'Urville to Dome C are calculated asymptotic  $\delta^{15}\text{N}(\text{NO}_3^-)$  values from Erbland et al. (2013) and Frey et al. (2009), which are representative of snow depths well below the photic zone at Dome C. The  $\delta^{15}\text{N}(\text{NO}_3^-)$  values along the transect from Dome A towards Zhongshan are asymptotic  $\delta^{15}\text{N}(\text{NO}_3^-)$  values calculated in Shi et al. (2014). The  $\delta^{15}\text{N}(\text{NO}_3^-)$  values at WAIS-Divide (Sofen et al., 2014) and South Pole (Jarvis, 2008) are average ice-core  $\delta^{15}\text{N}(\text{NO}_3^-)$  measurements from 1900–2000 CE, which are also representative of  $\delta^{15}\text{N}(\text{NO}_3^-)$  values well below the snow photic zone. Model-calculated ice-core  $\delta^{15}\text{N}(\text{NO}_3^-)$  values range from 0 to 363‰. The magnitude and spatial patterns of modeled ice-core  $\delta^{15}\text{N}(\text{NO}_3^-)$  compare well to observations, which range from 8 to 449‰. The modeled  $\delta^{15}\text{N}(\text{NO}_3^-)$  values are generally higher than observations, however, boundary layer  $\delta^{15}\text{N}(\text{NO}_3^-)$  observations are negative over much of Antarctica (Erbland et al., 2013; Frey et al., 2009; Morin et al., 2009; Savarino et al., 2007), making modeled  $\delta^{15}\text{N}(\text{NO}_3^-)$  values biased high by up to ~40‰. Both the modeled

<a href="#">Title Page</a>	
<a href="#">Abstract</a>	<a href="#">Introduction</a>
<a href="#">Conclusions</a>	<a href="#">References</a>
<a href="#">Tables</a>	<a href="#">Figures</a>
<a href="#">◀</a>	<a href="#">▶</a>
<a href="#">◀</a>	<a href="#">▶</a>
<a href="#">Back</a>	<a href="#">Close</a>
<a href="#">Full Screen / Esc</a>	
<a href="#">Printer-friendly Version</a>	
<a href="#">Interactive Discussion</a>	



and observed  $\delta^{15}\text{N}(\text{NO}_3^-)$  values show that  $\delta^{15}\text{N}(\text{NO}_3^-)$  is most enriched on the East Antarctic plateau, where the fraction of  $\text{NO}_3^-$  lost from the snow through photolysis is highest. In particular, the model largely captures the spatial gradient seen in the East Antarctic transect shown in Fig. 9b. The good agreement between modeled and observed  $\delta^{15}\text{N}(\text{NO}_3^-)$  suggests that its spatial pattern across the Antarctic continent is determined mainly by photolysis-driven loss of snow  $\text{NO}_3^-$ , due to the large nitrogen isotope fractionation effect associated with photolysis.

### 3.6 Relationship between nitrogen recycling and photolytic-loss of $\text{NO}_3^-$ in snow

- The degree of photolysis-driven loss of snow  $\text{NO}_3^-$  is determined by both rates of photolysis and transport patterns across the Antarctic continent. The spatial patterns of recycling ( $\text{NRF}_{\tau_z}$ , Fig. 7c) and loss ( $f$ , Fig. 9a) are generally similar; the highest degree of nitrogen recycling is located in regions with the highest fraction of photolysis-driven loss of  $\text{NO}_3^-$  in snow, such as in East Antarctica. Figure 10 shows the relationship between  $f$  and  $\ln(\text{NRF}_{\tau_z})$  across East and West Antarctica. There is a statistically-significant correlation between  $f$  and  $\ln(\text{NRF}_{\tau_z})$  in both East ( $r^2 = 0.88, p < 0.001$ ) and West ( $r^2 = 0.75, p < 0.001$ ) Antarctica. Despite the strong correlation between  $f$  and  $\text{NRF}_{\tau_z}$  across Antarctica, there are still locations where the magnitude of recycling and loss differ. For example, the average summer (DJF) flux of  $\text{NO}_x$  from the snow at Kohnen Station ( $75.0^\circ \text{S}, 0.0^\circ \text{E}$ ,  $\overline{F_{\text{NO}_x}} = 7.6 \times 10^8 \text{ molec cm}^{-2} \text{ s}^{-1}$ ) and Siple Dome ( $81.4^\circ \text{S}, 148.5^\circ \text{W}$ ,  $\overline{F_{\text{NO}_x}} = 5.9 \times 10^8 \text{ molec cm}^{-2} \text{ s}^{-1}$ ) are similar. The degree of nitrogen recycling is similar at Kohnen ( $\text{NRF}_{\tau_z} = 30$ ) and Siple Dome ( $\text{NRF}_{\tau_z} = 27$ ) as well, but the fraction of  $\text{NO}_3^-$  lost from the snow through photolysis is 0.99 at Kohnen and 0.73 at Siple Dome. This difference is driven by differences in transport between the two regions. Snow-sourced  $\text{NO}_x$  at Kohnen is transported downslope via katabatic winds, while Siple Dome is located near the Ross Ice Shelf convergence zone. The difference

<a href="#">Title Page</a>	
<a href="#">Abstract</a>	<a href="#">Introduction</a>
<a href="#">Conclusions</a>	<a href="#">References</a>
<a href="#">Tables</a>	<a href="#">Figures</a>
<a href="#">◀</a>	<a href="#">▶</a>
<a href="#">◀</a>	<a href="#">▶</a>
<a href="#">Back</a>	<a href="#">Close</a>
<a href="#">Full Screen / Esc</a>	
<a href="#">Printer-friendly Version</a>	
<a href="#">Interactive Discussion</a>	



in  $f$  (by 0.26) results in vast differences in modeled ice-core  $\delta^{15}\text{N}(\text{NO}_3^-)$  at Kohnen (226‰) and Siple Dome (64‰). However, since the magnitude of recycling and loss are correlated across most of Antarctica, and ice-core  $\delta^{15}\text{N}(\text{NO}_3^-)$  is mainly determined by the fractional loss of snow  $\text{NO}_3^-$ , observations of  $\delta^{15}\text{N}(\text{NO}_3^-)$  in snow and ice can be used to estimate both the degree of recycling and loss of snow  $\text{NO}_3^-$  across most of Antarctica, which can be useful for the interpretation of ice-core  $\text{NO}_3^-$ .

## 4 Conclusions

We have incorporated the photolysis of snow  $\text{NO}_3^-$  into a global chemical transport model (GEOS-Chem) for the first time in order to calculate the flux and redistribution of nitrogen in Antarctic snowpack. An important goal of this study is to investigate the impact of snowpack  $\text{NO}_3^-$  photolysis on boundary layer chemistry and the preservation of  $\text{NO}_3^-$  concentration and isotopes in Antarctic ice cores.

The calculated flux of snow-sourced  $\text{NO}_x$  from Antarctic snow ( $0.5\text{--}7.8 \times 10^8 \text{ molec cm}^{-2} \text{ s}^{-1}$ ) is in general agreement with snow  $\text{NO}_x$ -flux observations when using a quantum yield for snow  $\text{NO}_3^-$  photolysis on the order of  $10^{-3} \text{ molec photon}^{-1}$  (Chu and Anastasio, 2003). The flux of snow-sourced  $\text{NO}_x$  is overestimated by 2–3 orders of magnitude when the quantum yield from Zhu et al. (2010) is used along with various assumptions for the amount of photolabile  $\text{NO}_3^-$ . The modeled spatial pattern of the flux of snow-sourced  $\text{NO}_x$  is determined by the patterns of snow accumulation rate and light-absorbing impurity concentration across Antarctica. Snow-sourced  $\text{NO}_x$  is subject to transport across Antarctica, and recycled  $\text{NO}_3^-$  makes up a large fraction of the downward  $\text{NO}_3^-$  flux across the Antarctic continent, especially in regions of convergence over the Ronne, Ross, and Amery ice shelves.

The inclusion of snow-sourced  $\text{NO}_x$  in GEOS-Chem leads to factor increases in boundary layer mixing ratios for  $\text{NO}_x$  ranging from 7.0–31.6, gas and aerosol phase nitrate ranging from 3.9–38.1, OH ranging from 3.6–6.7, and  $\text{O}_3$  ranging from 1.3–2.0.

<a href="#">Title Page</a>	
<a href="#">Abstract</a>	<a href="#">Introduction</a>
<a href="#">Conclusions</a>	<a href="#">References</a>
<a href="#">Tables</a>	<a href="#">Figures</a>
<a href="#">◀</a>	<a href="#">▶</a>
<a href="#">◀</a>	<a href="#">▶</a>
<a href="#">Back</a>	<a href="#">Close</a>
<a href="#">Full Screen / Esc</a>	
<a href="#">Printer-friendly Version</a>	
<a href="#">Interactive Discussion</a>	



The incorporation of additional snow photochemical reactions into GEOS-Chem will also impact oxidant abundances, but the effects of each photochemical reaction will not be additive due to the highly non-linear nature of oxidant cycling.

The Nitrogen Recycling Factor (NRF<sub>year</sub>) ranges from 0.07 to 15.8, suggesting that nitrogen is recycled multiple times on average over the course of one year across all of Antarctica, except at the coasts where snow accumulation rates are high. Nitrate can remain in the photic zone for up to 7.5 years in Antarctic snow and is recycled multiple times (up to 57, on average) before burial beneath the photic zone in Antarctica. Along the Antarctic coast, the NRF<sub>T<sub>2</sub></sub> is less than 1, which suggests that ice-core NO<sub>3</sub><sup>-</sup> is relatively well preserved in coastal regions. The fraction of NO<sub>3</sub><sup>-</sup> lost from the snow through photolysis ranges from -0.21 to 0.99, where negative values indicate net gain of NO<sub>3</sub><sup>-</sup> to the snow. Photolysis of snow NO<sub>3</sub><sup>-</sup> results in a net gain of NO<sub>3</sub><sup>-</sup> in parts of West Antarctica, such as near the Ronne Ice Shelf where winds converge. The fraction of NO<sub>3</sub><sup>-</sup> lost from the snow through photolysis is highest on the East Antarctic plateau. The fraction of NO<sub>3</sub><sup>-</sup> lost from the snow through photolysis is used to calculate the enrichment in ice-core δ<sup>15</sup>N(NO<sub>3</sub><sup>-</sup>) solely from photolysis-driven NO<sub>3</sub><sup>-</sup> loss in snow. The modeled enrichment in ice-core δ<sup>15</sup>N(NO<sub>3</sub><sup>-</sup>) ranges from 0 to 363‰ and are in agreement with the magnitude and spatial patterns of observed sub-photocline δ<sup>15</sup>N(NO<sub>3</sub><sup>-</sup>) observations. The agreement between observed and modeled δ<sup>15</sup>N(NO<sub>3</sub><sup>-</sup>) suggests that its spatial variability across the Antarctic continent is determined by the degree of photolysis-driven loss of snow NO<sub>3</sub><sup>-</sup>. The variability in the spatial patterns of nitrogen recycling and photolysis-driven NO<sub>3</sub><sup>-</sup> loss in snow are broadly consistent across much of Antarctica, suggesting that ice-core δ<sup>15</sup>N(NO<sub>3</sub><sup>-</sup>) measurements can be used to examine the degree of nitrogen recycling in addition to NO<sub>3</sub><sup>-</sup> loss in most of Antarctica.

This is the first modeling study to incorporate snow NO<sub>3</sub><sup>-</sup> photolysis into a global chemical transport model to investigate the impacts of a snow-NO<sub>x</sub> source on boundary layer chemistry and nitrogen recycling and redistribution across Antarctica. Model

[Title Page](#)[Abstract](#)[Introduction](#)[Conclusions](#)[References](#)[Tables](#)[Figures](#)[|◀](#)[▶|](#)[◀](#)[▶](#)[Back](#)[Close](#)[Full Screen / Esc](#)[Printer-friendly Version](#)[Interactive Discussion](#)

- results shown here are broadly consistent with observations of the flux of  $\text{NO}_x$  from the Antarctic snowpack and snow  $\delta^{15}\text{N}(\text{NO}_3^-)$ , suggesting that the model captures the large-scale features of nitrogen recycling and loss across the Antarctic continent. Model sensitivity studies suggest that the flux of snow-sourced  $\text{NO}_x$  and loss of snow  $\text{NO}_3^-$
- 5 is most sensitive to the quantum yield for  $\text{NO}_3^-$  photolysis and the concentration of photolabile  $\text{NO}_3^-$ , which are likely related to one another. We suggest that future field, laboratory, and modeling studies continue to focus on gaining a better understanding of the quantum yield for  $\text{NO}_3^-$  photolysis and the concentration of photolabile  $\text{NO}_3^-$ , which will allow for the examination of nitrogen recycling on a molecular scale. Updated information
- 10 about the quantum yield for  $\text{NO}_3^-$  photolysis and the concentration of photolabile  $\text{NO}_3^-$  in snow along with additional snow photochemical reactions can be incorporated into this modeling framework in the future, which will continue to improve our understanding of the impacts of snow photochemistry on boundary layer chemistry and the preservation of  $\text{NO}_3^-$  and other photochemically-active impurities in ice cores.
- 15 **Acknowledgements.** We acknowledge support from NSF PLR 1244817, NSF PLR 0944537, NSF PLR 1446904, and an EPA STAR graduate fellowship to M. C. Zatko. The authors thank Steve Warren, Sarah Doherty, Thomas Grenfell, and Quentin Libois for helpful discussions about light absorbing impurities in snow and their influence of snow photochemistry. We thank Joseph Erbland for many helpful comments and discussions about nitrogen recycling. We also
- 20 thank Paul Hezel and Yanxu Zhang for helping M.C. Zatko learn GEOS-Chem. Lastly, we thank Qianjie Chen for helpful feedback on paper drafts and Martin Schneebeli for providing useful advice about snow grain profiles in Antarctic snow.

## References

- Alexander, B., Savarino, J., Kreutz, K. J., and Thieme, M. H.: Impact of preindustrial biomass burning emissions on the oxidation pathways of tropospheric sulphur and nitrogen, *J. Geophys. Res.*, 109, D08303, doi:10.1029/2003JD004218, 2004.

<a href="#">Title Page</a>	
<a href="#">Abstract</a>	<a href="#">Introduction</a>
<a href="#">Conclusions</a>	<a href="#">References</a>
<a href="#">Tables</a>	<a href="#">Figures</a>
<a href="#">◀</a>	<a href="#">▶</a>
<a href="#">◀</a>	<a href="#">▶</a>
<a href="#">Back</a>	<a href="#">Close</a>
<a href="#">Full Screen / Esc</a>	
<a href="#">Printer-friendly Version</a>	
<a href="#">Interactive Discussion</a>	



- Allen, D., Pickering, K., Duncan, B., and Damon, M.: Impact of lightning NO emissions on North American photochemistry as determined using the Global Modeling Initiative (GMI) model, *J. Geophys. Res.*, 115, D22301, doi:10.1029/2010JD014062, 2010.
- Amos, H. M., Jacob, D. J., Holmes, C. D., Fisher, J. A., Wang, Q., Yantosca, R. M., Corbitt, E. S., Galarneau, E., Rutter, A. P., Gustin, M. S., Steffen, A., Schauer, J. J., Graydon, J. A., Louis, V. L. St., Talbot, R. W., Edgerton, E. S., Zhang, Y., and Sunderland, E. M.: Gas-particle partitioning of atmospheric Hg(II) and its effect on global mercury deposition, *Atmos. Chem. Phys.*, 12, 591–603, doi:10.5194/acp-12-591-2012, 2012.
- Anastasio, C. and Chu, L.: Photochemistry of nitrous acid (HONO) and nitrous acidium ion ( $\text{H}_2\text{ONO}^+$ ) in aqueous solution and ice, *Environ. Sci. Technol.*, 43, 1108–1114, 2009.
- Anastasio, C., Galbavy, E. S., Hutterli, M. A., Burkhardt, J. F., and Friel, D. K.: Photoformation of hydroxyl radical on snow grains at Summit, Greenland, *Atmos. Environ.*, 41, 5110–5121, doi:10.1016/j.atmosenv.2006.12.011, 2007.
- Bauguitte, S. J.-B., Bloss, W. J., Evans, M. J., Salmon, R. A., Anderson, P. S., Jones, A. E., Lee, J. D., Saiz-Lopez, A., Roscoe, H. K., Wolff, E. W., and Plane, J. M. C.: Summertime  $\text{NO}_x$  measurements during the CHABLIS campaign: can source and sink estimates unravel observed diurnal cycles?, *Atmos. Chem. Phys.*, 12, 989–1002, doi:10.5194/acp-12-989-2012, 2012.
- Beine, H., Anastasio, C., Esposito, G., Patten, K., Wilkening, E., Domine, F., Voisin, D., Barret, M., Houdier, S., and Hall, S.: Soluble, light-absorbing species in snow at Barrow, Alaska, *J. Geophys. Res.*, 116, D00R05, doi:10.1029/2011JD016181, 2011.
- Berhanu, T. A., Meusinger, C., Erbland, J., Jost, R., Bhattacharya, S. K., Johnson, M. S., and Savarino, J.: Laboratory study of nitrate photolysis in Antarctic snow. II. Isotopic effects and wavelength dependence, *J. Chem. Phys.*, 140, 244306, doi:10.1063/1.4882899, 2014.
- Bertler, N., Mayewski, P. A., Aristarain, A., Barrett, P., Becagli, S., Bernardo, R., Bo, S., Xiao, C., Curran, M., Qin, D., Dixon, D., Ferron, F., Fischer, H., Frey, M., Frezzotti, M., Fundel, F., Gentthon, C., Gragnani, R., Hamilton, G., Handley, M., Hong, S., Isaksson, E., Kang, J., Ren, J., Kamiyama, K., Kanamori, S., Karkas, E., Karlof, L., Kaspari, S., Kreutz, K., Kurbatov, A., Meyerson, E., Ming, Y., Zhang, M., Motoyama, H., Mulvaney, R., Oerter, H., Osterberg, E., Proposito, M., Pyne, A., Ruth, U., Simoes, J., Smith, B., Snead, S., Teinila, K., Traufetter, F., Udisti, R., Virkkula, A., Watanabe, O., Williamson, R., Winther, J- G., Li, Y., Wolff, E., Li, Z., and Zielinski, A.: Snow chemistry across Antarctica, *Ann. Glaciol.*, 41, 167–179, 2005.

[Title Page](#)[Abstract](#)[Introduction](#)[Conclusions](#)[References](#)[Tables](#)[Figures](#)[◀](#)[▶](#)[◀](#)[▶](#)[Back](#)[Close](#)[Full Screen / Esc](#)[Printer-friendly Version](#)[Interactive Discussion](#)

- Bey, I., Jacob, D. J., Yantosca, R. M., Logan, J. A., Field, B. D., Fiore, A. M., Li, Q., Liu, H. Y., Mickley, L. J., and Schultz, M. G.: Global modeling of tropospheric chemistry with assimilated meteorology: model description and evaluation, *J. Geophys. Res.*, 106, 23073–23095, 2001.
- Bian, H. S. and Prather, M. J.: Fast-J2: Accurate simulation of stratospheric photolysis in global chemical models, *J. Atmos. Chem.*, 41, 281–296, 2002.
- Bisiaux, M. M., Edwards, R., McConnell, J. R., Curran, M. A. J., Van Ommen, T. D., Smith, A. M., Neumann, T. A., Pasteris, D. R., Penner, J. E., and Taylor, K.: Changes in black carbon deposition to Antarctica from two high-resolution ice core records, 1850–2000 AD, *Atmos. Chem. Phys.*, 12, 4107–4115, doi:10.5194/acp-12-4107-2012, 2012.
- Bloss, W. J., Lee, J. D., Heard, D. E., Salmon, R. A., Bauguitte, S. J.-B., Roscoe, H. K., and Jones, A. E.: Observations of OH and HO<sub>2</sub> radicals in coastal Antarctica, *Atmos. Chem. Phys.*, 7, 4171–4185, doi:10.5194/acp-7-4171-2007, 2007.
- Blunier, T., Gregoire, F. L., Jacobi, H.-W., and Quansah, E.: Isotopic view on nitrate loss in Antarctic surface snow, *Geophys. Res. Lett.*, 32, L13501, doi:10.1029/2005GL023011, 2005.
- Boxe, C. S., Colussi, A. J., Hoffmann, M. R., Murphy, J. G., Wolldridge, P. J., Bertram, T. H., and Cohen, R. C.: Photochemical production and release of gaseous NO<sub>2</sub> from nitrate-doped water ice, *J. Phys. Chem. A*, 109, 8520–8525, 2005.
- Casasanta, G., Pietroni, I., Petenko, I., and Argentini, S.: Observed and modelled convective mixing-layer height and Dome C, Antarctica, *Bound.-Lay. Meteorol.*, 151, 597–608, doi:10.1007/s10546-014-9907-5, 2014.
- Chen, G., Davis, D., Crawford, J., Hutterli, L. M., Huey, L. G., Slusher, D., Mauldin, L., Eisele, F., Tanner, D., Dibb, J., Buhr, M., McConnell, J., Lefer, B., Shetter, R., Blake, D., Song, C. H., Lombardi, K., and Arnoldy, J.: A reassessment of HO<sub>x</sub> South Pole chemistry based on observations recorded during ISCAT 2000, *Atmos. Environ.*, 38, 5451–5461, 2004.
- Cho, H., Shepson, P. B., Barrie, L. A., Cowin, J. P., and Zaveri, R.: NMR investigation of the quasi-brine layer in ice/brine mixtures, *J. Phys. Chem. B.*, 106, 11226–11232, 2002.
- Chu, L. and Anastasio, C.: Quantum yields of hydroxyl radicals and nitrogen dioxide from the photolysis of nitrate on ice, *J. Phys. Chem. A*, 107, 9594–9602, 2003.
- Chylek, P., Johnson, B., and Wu, H.: Black carbon concentration in Byrd station ice core – from 13 000 to 700 years before present, *Ann. Geophys.*, 10, 625–629, 1992, <http://www.ann-geophys.net/10/625/1992/>.

## The impact of snow nitrate photolysis in Antarctica

M. C. Zatko et al.

[Title Page](#)

[Abstract](#)

[Introduction](#)

[Conclusions](#)

[References](#)

[Tables](#)

[Figures](#)

◀

▶

◀

▶

[Back](#)

[Close](#)

[Full Screen / Esc](#)

[Printer-friendly Version](#)

[Interactive Discussion](#)



- Davis, D., Chen, G., Buhr, M., Crawford, J., Lenschow, D., Lefer, B., Shetter, R., Eisele, F., Mauldin, L., and Hogan, A.: South Pole NO<sub>x</sub> chemistry: an assessment of factors controlling variability and absolute levels, *Atmos. Environ.*, 38, 5375–5388, 2004.
- 5 Davis, D. D., Seelig, J., Huey, G., Crawford, J., Chen, G., Wang, Y., Buhr, M., Helmig, D., Neff, W., Blake, D., Arimoto, R., and Eisele, F.: A reassessment of Antarctic plateau reactive nitrogen based on ANTCI 2003 airborne and ground based measurements, *Atmos. Environ.*, 42, 2831–2848, doi:10.1016/j.atmosenv.2007.07.039, 2008.
- Dibb, J. E., Huey, G. L., Slusher, D. L., and Tanner, D. J.: Soluble reactive nitrogen oxides at South Pole during ISCAT 2000, *Atmos. Environ.*, 38, 5399–5409, 2004.
- 10 Doherty, S. J., Warren, S. G., Grenfell, T. C., Clarke, A. D., and Brandt, R. E.: Light-absorbing impurities in Arctic snow, *Atmos. Chem. Phys.*, 10, 11647–11680, doi:10.5194/acp-10-11647-2010, 2010.
- Doherty, S. J., Grenfell, T. C., Forsstrom, S., Hegg, D. L., Brandt, R. E., and Warren, S. G.: Observed vertical redistribution of black carbon and other insoluble light-absorbing particles in melting snow, *J. Geophys. Res.-Atmos.*, 118, 5553–5569, doi:10.1002/jgrd.50235, 2013.
- 15 Domine, F. and Shepson, P. B.: Air-snow interactions and atmospheric chemistry, *Science*, 297, 1506–1510, 2002.
- Domine, F., Bock, J., Voisin, D., and Donaldson, D. J.: Can we model snow photochemistry? Problems with the current approaches, *J. Phys. Chem. A*, 117, 4733–4749, doi:10.1021/jp3123314, 2013.
- 20 Erland, J., Vicars, W. C., Savarino, J., Morin, S., Frey, M. M., Frosini, D., Vince, E., and Martins, J. M. F.: Air–snow transfer of nitrate on the East Antarctic Plateau – Part 1: Isotopic evidence for a photolytically driven dynamic equilibrium in summer, *Atmos. Chem. Phys.*, 13, 6403–6419, doi:10.5194/acp-13-6403-2013, 2013.
- 25 Erland, J., Savarino, J., Morin, S., France, J. L., Frey, M. M., and King, M. D.: Airsnow transfer of nitrate on the East Antarctic plateau – Part 2: An isotopic model for the interpretation of deep ice-core records, *Atmos. Chem. Phys. Discuss.*, 15, 6887–6966, doi:10.5194/acpd-15-6887-2015, 2015.
- Fisher, J. A., Jacob, D. J., Wang, Q., Bahreini, R., Carouge, C. C., Cubison, M. J., Dibb, J. E., Diehl, T., Jimenez, J. L., Leibensperger, E. M., Meinders, M. B. T., Pye, H. O. T., Quinn, P. K., Sharma, S., van Donkelaar, A., and Yantosca, R. M.: Sources, distribution, and acidity of sulfate-ammonium aerosol in the Arctic in winter-spring, *Atmos. Environ.*, 45, 7301–7318, 2011.

[Title Page](#)[Abstract](#)[Introduction](#)[Conclusions](#)[References](#)[Tables](#)[Figures](#)[◀](#)[▶](#)[◀](#)[▶](#)[Back](#)[Close](#)[Full Screen / Esc](#)[Printer-friendly Version](#)[Interactive Discussion](#)

- Frey, M. M., Savarino, J., Morin, S., Erbland, J., and Martins, J. M. F.: Photolysis imprint in the nitrate stable isotope signal in snow and atmosphere of East Antarctica and implications for reactive nitrogen cycling, *Atmos. Chem. Phys.*, 9, 8681–8696, doi:10.5194/acp-9-8681-2009, 2009.
- 5 Frey, M. M., Brough, N., France, J. L., Anderson, P. S., Traulle, O., King, M. D., Jones, A. E., Wolff, E. W., and Savarino, J.: The diurnal variability of atmospheric nitrogen oxides (NO and NO<sub>2</sub>) above the Antarctic Plateau driven by atmospheric stability and snow emissions, *Atmos. Chem. Phys.*, 13, 3045–3062, doi:10.5194/acp-13-3045-2013, 2013.
- 10 Freyer, H. D., Kley, D., Voiz-Thomas, A., and Kobel, K.: On the interaction of isotopic exchange processes with photochemical reactions in atmospheric oxides of nitrogen, *J. Geophys. Res.-Atmos.*, 98, 14791–14796, 1993.
- 15 Gallet, J.-C., Domine, F., Arnaud, L., Picard, G., and Savarino, J.: Vertical profile of the specific surface area and density of the snow at Dome C and on a transect to Dumont D'Urville, Antarctica – albedo calculations and comparison to remote sensing products, *The Cryosphere*, 5, 631–649, doi:10.5194/tc-5-631-2011, 2011.
- Geng, L., Alexander, B., Cole-Dai, J., Steig, E. J., Savarino, J., Sofen, E. D., and Schauer, A. J.: 20 Nitrogen isotopes in ice core nitrate linked to anthropogenic atmospheric acidity change, *P. Natl. Acad. Sci.*, 111, 5808–5812, doi:10.1073/pnas.1319441111, 2014a.
- Geng, L., Cole-Dai, J., Alexander, B., Erbland, J., Savarino, J., Schauer, A. J., Steig, E. J., Lin, 25 P., Fu, Q., and Zatko, M. C.: On the origin of the occasional spring nitrate peak in Greenland snow, *Atmos. Chem. Phys.*, 14, 13361–13376, doi:10.5194/acp-14-13361-2014, 2014b.
- Grannas, A. M., Jones, A. E., Dibb, J., Ammann, M., Anastasio, C., Beine, H. J., Bergin, M., Bottenheim, J., Boxe, C. S., Carver, G., Chen, G., Crawford, J. H., Dominé, F., Frey, M. M., Guzmán, M. I., Heard, D. E., Helmig, D., Hoffmann, M. R., Honrath, R. E., Huey, L. G., Hutterli, M., Jacobi, H. W., Klán, P., Lefer, B., McConnell, J., Plane, J., Sander, R., Savarino, J., Shepson, P. B., Simpson, W. R., Sodeau, J. R., von Glasow, R., Weller, R., Wolff, E. W., and Zhu, T.: An overview of snow photochemistry: evidence, mechanisms and impacts, *Atmos. Chem. Phys.*, 7, 4329–4373, doi:10.5194/acp-7-4329-2007, 2007.
- Grenfell, T. C.: A radiative transfer model for sea ice with vertical structure variations, *J. Geophys. Res.*, 96, 16991–17001, 1991.
- Grenfell, T. C., Warren, S. G., and Mullen, P. C.: Reflection of solar radiation by the Antarctic snow surface at ultraviolet, visible, and near-infrared wavelengths, *J. Geophys. Res.*, 99, 18669–18684, 1994.

<a href="#">Title Page</a>	<a href="#">Abstract</a>	<a href="#">Introduction</a>
<a href="#">Conclusions</a>	<a href="#">References</a>	
<a href="#">Tables</a>	<a href="#">Figures</a>	
<a href="#">◀</a>	<a href="#">▶</a>	
<a href="#">◀</a>	<a href="#">▶</a>	
<a href="#">Back</a>	<a href="#">Close</a>	
<a href="#">Full Screen / Esc</a>		
	<a href="#">Printer-friendly Version</a>	
	<a href="#">Interactive Discussion</a>	



## The impact of snow nitrate photolysis in Antarctica

M. C. Zatko et al.

[Title Page](#)

[Abstract](#)

[Introduction](#)

[Conclusions](#)

[References](#)

[Tables](#)

[Figures](#)

◀

▶

◀

▶

[Back](#)

[Close](#)

[Full Screen / Esc](#)

[Printer-friendly Version](#)

[Interactive Discussion](#)



- Handorf, D., Foken, T., and Kottmeier, C.: The stable atmospheric boundary layer over an Antarctic ice sheet, *Bound.-Lay. Meteorol.*, 91, 165–189, 1999.
- Hastings, M. G., Sigman, D. M., and Steig, E. J.: Glacial/interglacial changes in the isotopes of nitrate from the Greenland Ice Sheet Project (GISP2) ice core, *Global Biogeochem. Cy.*, 19, GB4024, doi:10.1029/2005GB002502, 2005.
- Heaton, T. H. E., Spiro, B., and Robertson, M. C. S.: Potential canopy influences on the isotopic composition of nitrogen and sulphur in atmospheric deposition, *Oecologia*, 109, 600–607, 1997.
- 10 Helming, D., Johnson, B., Oltmans, S. J., Neff, W., Eisele, F., and Davis, D.: Elevated ozone in the boundary layer at South Pole, *Atmos. Environ.*, 42, 2788–2803, 2008.
- Holtslag, A. A. M. and Boville, B.: Local versus nonlocal boundary layer diffusion in a global climate model, *J. Climate*, 6, 1825–1842, 1993.
- 15 Hudman, R. C., Moore, N. E., Mebust, A. K., Martin, R. V., Russell, A. R., Valin, L. C., and Cohen, R. C.: Steps towards a mechanistic model of global soil nitric oxide emissions: implementation and space based-constraints, *Atmos. Chem. Phys.*, 12, 7779–7795, doi:10.5194/acp-12-7779-2012, 2012.
- Jarvis, J. C.: Isotopic Studies of Ice Core Nitrate and Atmospheric Nitrogen Oxides in Polar Regions, PhD thesis, University of Washington, USA, 2008.
- 20 Jones, A., Weller, R., Anderson, P., Jacobi, H., Wolff, E., Schrems, O., and Miller, H.: Measurements of  $\text{NO}_x$  emissions from the Antarctic snowpack, *Geophys. Res. Lett.*, 28, 1499–1502, doi:10.1029/2000GL011956, 2001.
- Jones, A. E., Anderson, P. S., Wolff, E. W., Turner, J., Rankin, A. M., and Colwell, S. R.: A role for newly forming sea ice in springtime polar tropospheric ozone loss? Observational evidence from Halley station, Antarctica, *J. Geophys. Res.*, 111, D08306, doi:10.1029/2005JD006566, 2006.
- 25 Jones, A. E., Wolff, E. W., Salmon, R. A., Bauguitte, S. J.-B., Roscoe, H. K., Anderson, P. S., Ames, D., Clemithshaw, K. C., Fleming, Z. L., Bloss, W. J., Heard, D. E., Lee, J. D., Read, K. A., Hamer, P., Shallcross, D. E., Jackson, A. V., Walker, S. L., Lewis, A. C., Mills, G. P., Plane, J. M. C., Saiz-Lopez, A., Sturges, W. T., and Worton, D. R.: Chemistry of the Antarctic Boundary Layer and the Interface with Snow: an overview of the CHABLIS campaign, *Atmos. Chem. Phys.*, 8, 3789–3803, doi:10.5194/acp-8-3789-2008, 2008.
- 30 Jones, A. E., Wolff, E. W., Ames, D., Bauguitte, S. J.-B., Clemithshaw, K. C., Fleming, Z., Mills, G. P., Saiz-Lopez, A., Salmon, R. A., Sturges, W. T., and Worton, D. R.: The multi-seasonal  $\text{NO}_y$

budget in coastal Antarctica and its link with surface snow and ice core nitrate: results from the CHABLIS campaign, *Atmos. Chem. Phys.*, 11, 9271–9285, doi:10.5194/acp-11-9271-2011, 2011.

King, J. C., Argentini, S. A., and Anderson, P. S.: Contrasts between the summertime surface energy balance and boundary layer structure at Dome C and Halley stations, Antarctica, *J. Geophys. Res.*, 111, D02105, doi:10.1029/2005JD006130, 2006.

Klein, K.: Variability in Dry Antarctic Firn; Investigations on Spatially Distributed Snow and Firn Samples from Dronning Maud Land, Antarctica, PhD thesis, Universität Bremen, Germany, available at: <http://nbn-resolving.de/urn:nbn:de:gbv:46-00104117-15>, last access: 15 April 2014.

Kodama, Y., Wendler, G., and Ishikawa, N.: The diurnal variation of the boundary layer in summer in Adelie Land, Eastern Antarctica, *J. Appl. Meteorol.*, 28, 16–24, 1989.

Konig-Langlo, G., King, J., and Pettre, P.: Climatology of the three coastal Antarctic stations Dumont D'Urville, Neumayer, and Halley, *J. Geophys. Res.*, 103, 10935–10946, 1998.

Lee, H., Henze, D. K., Alexander, B., and Murray, L. T.: Investigating the sensitivity of surface-level nitrate seasonality in Antarctica to primary sources using a global model, *Atmos. Environ.*, 89, 757–767, doi:10.1016/j.atmosenv.2014.03.003, 2014.

Levy, H., Moxim, W. J., Klonecki, A. A., and Kasibhatla, P. S.: Simulated tropospheric NO<sub>x</sub>: its evaluation, global distribution and individual source contributions, *J. Geophys. Res.*, 104, 26279–26306, 1999.

Libois, Q., Picard, G., France, J. L., Arnaud, L., Dumont, M., Carmagnola, C. M., and King, M. D.: Influence of grain shape on light penetration in snow, *The Cryosphere*, 7, 1803–1818, doi:10.5194/tc-7-1803-2013, 2013.

Liu, H., Jacob, D. J., Bey, I., and Yantosca, R. M.: Constraints from <sup>210</sup>Pb and <sup>7</sup>Be on wet deposition and transport in a global three-dimensional chemical tracer model driven by assimilated meteorological fields, *J. Geophys. Res.*, 106, 12109–12128, 2001.

Logan, J. A.: Nitrogen oxides in the troposphere: global and regional budgets, *J. Geophys. Res.*, 88, 10785–10807, doi:10.1029/JC088iC15p10785, 1983.

Mack, J. and Bolton, J. R.: Photochemistry of nitrite and nitrate in aqueous solution: a review, *J. Photoch. Photobio. A*, 128, 1–13, 1999.

Mao, J., Jacob, D. J., Evans, M. J., Olson, J. R., Ren, X., Brune, W. H., Clair, J. M. St., Crounse, J. D., Spencer, K. M., Beaver, M. R., Wennberg, P. O., Cubison, M. J., Jimenez, J. L., Fried, A., Weibring, P., Walega, J. G., Hall, S. R., Weinheimer, A. J., Co-

Title Page

Abstract

Introduction

Conclusions

References

Tables

Figures

◀

▶

◀

▶

Back

Close

Full Screen / Esc

Printer-friendly Version

Interactive Discussion



- hen, R. C., Chen, G., Crawford, J. H., McNaughton, C., Clarke, A. D., Jaeglé, L., Fisher, J. A., Yantosca, R. M., Le Sager, P., and Carouge, C.: Chemistry of hydrogen oxide radicals ( $\text{HO}_x$ ) in the Arctic troposphere in spring, *Atmos. Chem. Phys.*, 10, 5823–5838, doi:10.5194/acp-10-5823-2010, 2010.
- 5 Masclin, S., Frey, M. M., Rogge, W. F., and Bales, R. C.: Atmospheric nitric oxide and ozone at the WAIS Divide deep coring site: a discussion of local sources and transport in West Antarctica, *Atmos. Chem. Phys.*, 13, 8857–8877, doi:10.5194/acp-13-8857-2013, 2013.
- Mayewski, P. A. and Legrand, M. R.: Recent increase in nitrate concentration of Antarctic snow, *Nature*, 346, 258–260, 1990.
- 10 Meusinger, C., Berhanu, T. A., Erbland, J., Savarino, J., and Johnson, M. S.: Laboratory study of nitrate photolysis in Antarctic snow – Part 1: Observed quantum yield, domain of photolysis, and secondary chemistry, *J. Chem. Phys.*, 140, 244305, doi:10.1063/1.4882898, 2014.
- Morin, S., Savarino, J., Frey, M. M., Domine, F., Jacobi, H.-W., Kaleschke, L., and Martins, J. M. F.: Comprehensive isotopic composition of atmospheric nitrate in the Atlantic Ocean boundary layer from 65°S to 79°N, *J. Geophys. Res.*, 114, D05303, doi:10.1029/2008JD010696, 2009.
- 15 Mulvaney, R., Wagenbach, D., and Wolff, E. W.: Postdepositional change in snowpack nitrate from observation of year-round near-surface snow in coastal Antarctica, *J. Geophys. Res.*, 103, 11021–11031, 1998.
- 20 Murray, L. T., Jacob, D. J., Logan, J. A., Hudman, R. C., and Koshak, W. J.: Optimized regional and interannual variability of lightning in a global chemical transport model constrained by LIS/OTD satellite data, *J. Geophys. Res.*, 117, D20307, doi:10.1029/2012JD017934, 2012.
- Neff, W., Helming, D., Grachev, A., and Davis, D.: A study of boundary layer behaviour associated with high concentrations at the South Pole using a minisodder, tethered balloon, and a sonic anemometer, *Atmos. Environ.*, 42, 2762–2779, 2008.
- 25 Oliver, J. G. J., Van Aardenne, J. A., Dentener, F. J., Pagliari, V., Ganzeveld, L. N., and Peters, J. A. H. W.: Recent trends in global greenhouse gas emissions: regional trends 1970–2000 and spatial distribution of key sources in 2000, *Environm. Sci.*, 2, 81–99, doi:10.1080/15693430500400345, 2005.
- 30 Oncley, S., Buhr, M., Lenschow, D., Davis, D., and Semmer, S.: Observations of summertime NO fluxes and boundary-layer height at the South Pole during ISCAT 2000 using scalar similarity, *Atmos. Environ.*, 38, 5389–5398, doi:10.1016/j.atmosenv.2004.05.053, 2004.

## The impact of snow nitrate photolysis in Antarctica

M. C. Zatko et al.

[Title Page](#)

[Abstract](#)

[Introduction](#)

[Conclusions](#)

[References](#)

[Tables](#)

[Figures](#)

◀

▶

◀

▶

[Back](#)

[Close](#)

[Full Screen / Esc](#)

[Printer-friendly Version](#)

[Interactive Discussion](#)



The impact of snow nitrate photolysis in Antarctica

M. C. Zatko et al.

<a href="#">Title Page</a>	
<a href="#">Abstract</a>	<a href="#">Introduction</a>
<a href="#">Conclusions</a>	<a href="#">References</a>
<a href="#">Tables</a>	<a href="#">Figures</a>
<a href="#">◀</a>	<a href="#">▶</a>
<a href="#">◀</a>	<a href="#">▶</a>
<a href="#">Back</a>	<a href="#">Close</a>
<a href="#">Full Screen / Esc</a>	
<a href="#">Printer-friendly Version</a>	
<a href="#">Interactive Discussion</a>	



Parish, T. R. and Bromwich, D. H.: Reexamination of the near-surface airflow over the Antarctic continent and implications on atmospheric circulations at high southern latitudes, *Mon. Weather Rev.*, 135, 1961–1973, 2007.

Parrella, J. P., Jacob, D. J., Liang, Q., Zhang, Y., Mickley, L. J., Miller, B., Evans, M. J., Yang, X.,  
Pyle, J. A., Theys, N., and Van Roozendael, M.: Tropospheric bromine chemistry: implications for present and pre-industrial ozone and mercury, *Atmos. Chem. Phys.*, 12, 6723–6740,  
doi:10.5194/acp-12-6723-2012, 2012.

Pratt, K. A., Custard, K. D., Shepson, P. B., Douglas, T. A., Pohler, D., General, S., Zielcke, J.,  
Simpson, W. R., Platt, U., Tanner, D. J., Huey, L. G., Carlsen, M., and Stirm, B. H.: Photochemical production of molecular bromine in Arctic surface snowpacks, *Nature*, 6, 351–356,  
doi:10.1038/NGEO1779, 2013.

Price, C. and Rind, D.: A simple lightning parameterization for calculating global lightning distributions, *J. Geophys. Res.*, 97, 9919–9933, 1992.

Rothlisberger, R., Hutterli, M. A., Sommer, S., Wolff, E. W., and Mulvaney, R.: Factors controlling nitrate in ice cores: evidence from the Dome C deep ice core, *J. Geophys. Res.*, 105, 20565–20572, 2000.

Sander, S. P., Friedl, R. R., Golden, D. M., Kurylo, M. J., Moortgat, G. K., Keller-Rudek, H.,  
Wine, P. J., Ravishankara, A. R., Kolb, C. E., Molina, M. J., Finalyson-Pitts, B. J., Huie, R. E.,  
and Orkin, V. L.: Chemical kinetics and photochemical data for use in atmospheric studies evaluation number 15, JPL Publications, 06-2, Pasadena, California, USA, 1–523, 2006.

Savarino, J., Kaiser, J., Morin, S., Sigman, D. M., and Thiemens, M. H.: Nitrogen and oxygen isotopic constraints on the origin of atmospheric nitrate in coastal Antarctica, *Atmos. Chem. Phys.*, 7, 1925–1945, doi:10.5194/acp-7-1925-2007, 2007.

Shi, G., Buffen, A. M., Hastings, M. G., Li, C., Ma, H., Li, Y., Sun, B., An, C., and Jiang, S.: Investigation of post-depositional processing of nitrate in East Antarctic snow: isotopic constraints on photolytic loss, re-oxidation, and source inputs, *Atmos. Chem. Phys. Discuss.*, 14, 31943–31986, doi:10.5194/acpd-14-31943-2014, 2014.

Simpson, W. R., von Glasow, R., Riedel, K., Anderson, P., Ariya, P., Bottenheim, J., Burrows, J., Carpenter, L. J., Frieß, U., Goodsite, M. E., Heard, D., Hutterli, M., Jacobi, H.-W., Kaleschke, L., Neff, B., Plane, J., Platt, U., Richter, A., Roscoe, H., Sander, R., Shepson, P., Sodeau, J., Steffen, A., Wagner, T., and Wolff, E.: Halogens and their role in polar boundary-layer ozone depletion, *Atmos. Chem. Phys.*, 7, 4375–4418, doi:10.5194/acp-7-4375-2007, 2007.

- Sjostedt, S. J., Huey, L. G., Tanner, D. J., Peischl, J., Chen, G., Dibb, J. E., Lefer, B., Hutterli, M. A., Beyersdorf, A. J., Blake, N. J., Blake, D. R., Sueper, D., Ryerson, T., Burkhardt, J., and Stohl, A.: Observations of hydroxul and the sum of peroxy radicals at Summit, Greenland during summer 2003, *Atmos. Environ.*, 41, 5122–5137, 2007.
- Slusher, D. L., Huey, L. G., Tanner, D. J., Chen, G., Davis, D. D., Buhr, M., Nowak, J. B., Eisele, F. L., Kosciuch, E., Mauldin, R. L., Lefer, B. L., Shetter, R. E., and Dibb, J. E.: Measurements of pernitric acid at the South Pole during ISCAT 2000, *Geophys. Res. Lett.*, 29, 7–1–7–4, doi:10.1029/2002GL015703, 2002.
- 10 Sofen, E. D., Alexander, B., Steig, E. J., Thiemens, M. H., Kunasek, S. A., Amos, H. M., Schauer, A. J., Hastings, M. G., Bautista, J., Jackson, T. L., Vogel, L. E., McConnell, J. R., Pasteris, D. R., and Saltzman, E. S.: WAIS Divide ice core suggests sustained changes in the atmospheric formation pathways of sulfate and nitrate since the 19th century in the extratropical Southern Hemisphere, *Atmos. Chem. Phys.*, 14, 5749–5769, doi:10.5194/acp-14-5749-2014, 2014.
- 15 Thomas, J. L., Dibb, J. E., Huey, L. G., Liao, J., Tanner, D., Lefer, B., von Glasow, R., and Stutz, J.: Modeling chemistry in and above snow at Summit, Greenland – Part 2: Impact of snowpack chemistry on the oxidation capacity of the boundary layer, *Atmos. Chem. Phys.*, 12, 6537–6554, doi:10.5194/acp-12-6537-2012, 2012.
- 20 Thompson, A. M.: The oxidizing capacity of the Earth's atmosphere: probable past and future changes, *Science*, 256, 1157–1165, 1992.
- Travouillon, T., Ashley, M. C. B., Burton, M. G., Storey, J. W. V., and Loewenstein, R. F.: Atmospheric turbulence at the South Pole and its implications for astronomy, *Astron. Astrophys.*, 400, 1163–1172, doi:10.1051/0004-6361:20021814, 2003.
- 25 UNEP/WMO: Integrated Assessment of Black Carbon and Tropospheric Ozone: Summary for Decision Makers, UNON/Publishing Services Section, Nairobi, ISO 14001:2004, 2011.
- van der Werf, G. R., Morton, D. C., DeFries, R. S., Giglio, L., Randerson, J. T., Collatz, G. J., and Kasibhatla, P. S.: Estimates of fire emissions from an active deforestation region in the southern Amazon based on satellite data and biogeochemical modelling, *Biogeosciences*, 6, 235–249, doi:10.5194/bg-6-235-2009, 2009.
- 30 van Donkelaar, A., Martin, R. V., Leaitch, W. R., Macdonald, A. M., Walker, T. W., Streets, D. G., Zhang, Q., Dunlea, E. J., Jimenez, J. L., Dibb, J. E., Huey, L. G., Weber, R., and Andreae, M. O.: Analysis of aircraft and satellite measurements from the Intercontinental Chemical

[Title Page](#)

[Abstract](#)

[Introduction](#)

[Conclusions](#)

[References](#)

[Tables](#)

[Figures](#)

◀

▶

◀

▶

[Back](#)

[Close](#)

[Full Screen / Esc](#)

[Printer-friendly Version](#)

[Interactive Discussion](#)



Transport Experiment (INTEX-B) to quantify long-range transport of East Asian sulfur to Canada, *Atmos. Chem. Phys.*, 8, 2999–3014, doi:10.5194/acp-8-2999-2008, 2008.

- 5 Wang, Q., Jacob, D. J., Fisher, J. A., Mao, J., Leibensperger, E. M., Carouge, C. C., Le Sager, P., Kondo, Y., Jimenez, J. L., Cubison, M. J., and Doherty, S. J.: Sources of carbonaceous aerosols and deposited black carbon in the Arctic in winter-spring: implications for radiative forcing, *Atmos. Chem. Phys.*, 11, 12453–12473, doi:10.5194/acp-11-12453-2011, 2011.
- 10 Wang, Y., Choi, Y., Zeng, T., Davis, D., Buhr, M., Huey, G. L., and Neff, W.: Assessing the photochemical impact of snow NO<sub>x</sub> emissions over Antarctica during ANTCI 2003, *Atmos. Environ.*, 41, 3944–3958, doi:10.1016/j.atmosenv.2007.01.056, 2008.
- 15 Warren, S. G. and Clarke, A. D.: Soot in the atmosphere and snow surface of Antarctica, *J. Geophys. Res.*, 95, 1811–1816, 1990.
- 20 Warren, S. G., Brandt, R. E., and Grenfell, T. C.: Visible and near-ultraviolet absorption spectrum of ice from transmission of solar radiation into snow, *Appl. Optics*, 45, 5320–5334, 2006.
- 25 Weller, R., Minikin, A., Konig-Langlo, G., Schrems, O., Jones, A. E., Wolff, E. W., and Anderson, P. S.: Investigating possible causes of the observed diurnal variability in Antarctic NO<sub>y</sub>, *Geophys. Res. Lett.*, 26, 2853–2856, 1999.
- 30 Wesely, M. L.: Parameterization of surface resistances to gaseous dry deposition in regional-scale numerical-models, *Atmos. Environ.*, 23, 1293–130, 1989.
- Wild, O., Zhu, Q., and Prather, M. J.: Fast-J: accurate simulation of in- and below-cloud photolysis in global chemical models, *J. Atmos. Chem.*, 37, 245–282, 2000.
- 35 Wolff, E. W.: Nitrate in polar ice, in: *Ice Core Studies of Global Biogeochem. Cycles*, NATO ASI Ser., Ser. I, 195–224, edited by: Delmas, R. J., Springer, New York, USA, 1995.
- 40 Wolff, E. W., Jones, A. E., Bauguitte, S. J.-B., and Salmon, R. A.: The interpretation of spikes and trends in concentration of nitrate in polar ice cores, based on evidence from snow and atmospheric measurements, *Atmos. Chem. Phys.*, 8, 5627–5634, doi:10.5194/acp-8-5627-2008, 2008.
- 45 Zatko, M. C. and Warren, S. G.: East Antarctic sea ice in spring: spectral albedo of snow, nilas, frost flowers, and slush; and light-absorbing impurities in snow, *Ann. Glaciol.*, 56, 53–64, doi:10.3189/2015AoG69A574, 2015.

## The impact of snow nitrate photolysis in Antarctica

M. C. Zatko et al.

[Title Page](#)

[Abstract](#)

[Introduction](#)

[Conclusions](#)

[References](#)

[Tables](#)

[Figures](#)

[◀](#)

[▶](#)

[◀](#)

[▶](#)

[Back](#)

[Close](#)

[Full Screen / Esc](#)

[Printer-friendly Version](#)

[Interactive Discussion](#)



**The impact of snow nitrate photolysis in Antarctica**

M. C. Zatko et al.

[Title Page](#)[Abstract](#)[Introduction](#)[Conclusions](#)[References](#)[Tables](#)[Figures](#)[|◀](#)[▶|](#)[◀](#)[▶](#)[Back](#)[Close](#)[Full Screen / Esc](#)[Printer-friendly Version](#)[Interactive Discussion](#)

Zatko, M. C., Grenfell, T. C., Alexander, B., Doherty, S. J., Thomas, J. L., and Yang, X.: The influence of snow grain size and impurities on the vertical profiles of actinic flux and associated NO<sub>x</sub> emissions on the Antarctic and Greenland ice sheets, *Atmos. Chem. Phys.*, 13, 3547–3567, doi:10.5194/acp-13-3547-2013, 2013.

- 5 Zhang, L., Gong, S., Padro, J., and Barrie, L.: A size-segregated particle dry deposition scheme for an atmospheric aerosol module, *Atmos. Environ.*, 35, 549–560, 2001.  
Zhu, C., Xiang, B., Chu, L. T., and Zhu, L.: 308 nm photolysis of nitric acid in the gas phase, on aluminum surfaces, and on ice films, *J. Phys. Chem. A.*, 114, 2561–2568, doi:10.1021/jp909867a, 2010.

**Table 1.** Glossary of variables used in this paper.

Variable	Unit	Description
$\lambda$	nm	Wavelength
$\phi$	molec photon <sup>-1</sup>	Quantum yield for $\text{NO}_3^-$ photolysis
$\sigma_{\text{NO}_3^-}$	cm <sup>2</sup>	Absorption cross-section for $\text{NO}_3^-$ photolysis
$I$	photons cm <sup>-2</sup> s <sup>-1</sup> nm <sup>-1</sup>	Actinic flux of UV radiation
$Z_e$	cm	e-folding depth of UV actinic flux in snow
$Z_{3e}$	cm	Depth of snow photic zone
$\alpha_r$	kg m <sup>-2</sup> year <sup>-1</sup>	Total annual snow accumulation rate
$C_{\text{BC}}$	ng g <sup>-1</sup>	Annual mean snow black carbon concentration
$r_e$	μm	Radiation equivalent mean ice grain radii
$K_{\text{ext,tot}}$	cm <sup>-1</sup>	Bulk extinction coefficient for snow
$[\text{NO}_3^-]_{\text{top}}$	ng g <sup>-1</sup>	Mean $\text{NO}_3^-$ concentration in top 2 cm of snow
$[\text{NO}_3^-]_{\text{bot}}$	ng g <sup>-1</sup>	Mean $\text{NO}_3^-$ concentration in below 2 cm snow depth
EF	unitless	$\text{NO}_3^-$ enhancement factor in top 2 cm of snow
$F_p$	fraction	Fraction of photolabile $\text{NO}_3^-$ in snow
$\Delta^{17}\text{O}(\text{NO}_3^-)$	‰	Oxygen isotopic composition of $\text{NO}_3^-$
$\delta^{15}\text{N}(\text{NO}_3^-)$	‰	Nitrogen isotopic composition of $\text{NO}_3^-$
$\varepsilon$	‰	Fractionation constant for $\text{NO}_3^-$ photolysis
$F_{\text{NO}_x}$	molec cm <sup>-2</sup> s <sup>-1</sup>	Mean austral summer flux of snow-sourced $\text{NO}_x$
$F_{\text{NO}_x}$	ng N m <sup>-2</sup> year <sup>-1</sup>	Annual sum of snow-sourced $\text{NO}_x$ flux
$F_{\text{PRI}}$	ng N m <sup>-2</sup> year <sup>-1</sup>	Annual sum of primary $\text{NO}_3^-$ deposited to snow
$F_R$	ng N m <sup>-2</sup> year <sup>-1</sup>	Annual sum of recycled $\text{NO}_3^-$ to snow
$\text{NRF}_{\text{year}}$	unitless	Metric to assess degree of nitrogen recycling in 1 year
$\text{NRF}_{\tau_z}$	unitless	Metric to assess degree of nitrogen recycling before $\text{NO}_3^-$ burial below snow photic zone
$\tau_z$	years	Years $\text{NO}_3^-$ remains in snow photic zone
$f$	fraction	Fraction of photolysis-driven loss of $\text{NO}_3^-$ from snow

## The impact of snow nitrate photolysis in Antarctica

M. C. Zatko et al.

[Title Page](#)

[Abstract](#)

[Introduction](#)

[Conclusions](#)

[References](#)

[Tables](#)

[Figures](#)

◀

▶

[Back](#)

[Close](#)

[Full Screen / Esc](#)

[Printer-friendly Version](#)

[Interactive Discussion](#)



Title Page	
Abstract	Introduction
Conclusions	References
Tables	
Figures	
<a href="#">◀</a>	<a href="#">▶</a>
<a href="#">◀</a>	<a href="#">▶</a>
Back	Close
Full Screen / Esc	
Printer-friendly Version	
Interactive Discussion	

**Table 2.** Dependence of mean austral summer (DJF) flux of snow-sourced  $\text{NO}_x$  ( $\overline{F_{\text{NO}_x}}$ ) on quantum yield ( $\phi$ ), the fraction of photolabile  $\text{NO}_3^-$  ( $F_p$ ), snow  $\text{NO}_3^-$  concentrations below 2 cm ( $[\text{NO}_3^-]_{\text{bot}}$ ), the radiation equivalent ice grain radius ( $r_e$ ), the bulk snow extinction coefficient ( $K_{\text{ext,tot}}$ ), the  $\text{NO}_3^-$  concentration enhancement factor in the top 2 cm (EF), and snow black carbon concentrations ( $C_{\text{BC}}$ ).

Parameter	Base case values	Values used in sensitivity studies	Factor changes in $\overline{F_{\text{NO}_x}}$ compared to base case <sup>a</sup> ( $\overline{F_{\text{NO}_x}}$ range, units: $\times 10^8 \text{ molec cm}^{-2} \text{ s}^{-1}$ )
Quantum yield ( $\phi$ )	$1.0 \times 10^{-3} \text{ molec photon}^{-1}$ <sup>b</sup>	$0.6 \text{ molec photon}^{-1}$	10–333.0 (5–2600)
Fraction of photolabile $\text{NO}_3^-$ ( $F_p$ )	0.01–0.99 (spatial variation, Fig. 3c)	Set to 1 everywhere	1.2–7.4 (3.7–9.6)
Snow $\text{NO}_3^-$ below 2 cm ( $[\text{NO}_3^-]_{\text{bot}}$ )	$60.0 \text{ ng g}^{-1}$ <sup>c</sup>	$30\text{--}120 \text{ ng g}^{-1}$	0.6–2.0 (0.3–15.8)
Radiation equivalent mean ice grain radii ( $r_e$ )	Jan: $332.0 \mu\text{m}$ <sup>d</sup> Dec–Feb: $198\text{--}332.0 \mu\text{m}$ <sup>d</sup> Mar–Nov: $86.0\text{--}332.0 \mu\text{m}$ <sup>d</sup>	Study 1: $332.0 \mu\text{m}$ <sup>e</sup> Study 2: $198\text{--}332.0 \mu\text{m}$ <sup>e</sup> Study 3: $86.0\text{--}332.0 \mu\text{m}$ <sup>e</sup>	1.0–1.3 (0.5–10.2)
Bulk snow extinction coefficient ( $K_{\text{ext,tot}}$ )	$1.7\text{--}6.9 \times 10^3 \text{ m}^{-1}$ (spatial variation)	$\pm 20\%$ with respect to base case values	1.0–1.2 (0.5–9.4)
$\text{NO}_3^-$ enhancement factor in top 2 cm (EF)	$6.0^f$	1–10	1.0–1.2 (0.5–9.3)
Snow black carbon ( $C_{\text{BC}}$ )	$0.08\text{--}0.6 \text{ ng g}^{-1}$ (spatial variation, Fig. 3b)	$\pm$ factor of 2 with respect to base case values	1.0–1.1 (0.5–8.6)

<sup>a</sup> base case  $\overline{F_{\text{NO}_x}} = 0.5\text{--}7.8 \times 10^8 \text{ molec cm}^{-2} \text{ s}^{-1}$  (Fig. 4d).

<sup>b</sup> from Chu and Anastasio (2003).

<sup>c</sup> median of ITASE campaign (Bertler et al., 2005).

<sup>d</sup>  $r_e$  is varied vertically and temporally, but uniformly across Antarctica based on Gallet et al. (2011) and Klein (2014). In January,  $r_e$  is constant with depth (332  $\mu\text{m}$ ), in December and February,  $r_e$  ranges from 198  $\mu\text{m}$  at the snow surface to 332  $\mu\text{m}$  at 300 cm depth, and from March to November,  $r_e$  ranges from 86  $\mu\text{m}$  at the surface to 360  $\mu\text{m}$  at 300 cm depth.

<sup>e</sup> in  $r_e$  sensitivity study 1, the base-case “January”  $r_e$  profile is applied for every month. In  $r_e$  sensitivity study 2, the base-case “December and February”  $r_e$  profile is applied for every month. In  $r_e$  sensitivity study 3, the base-case “March–November”  $r_e$  profile is applied for every month.

<sup>f</sup> median of observed EF (Dibb et al., 2004; Frey et al., 2009; Mayewski and Legrand, 1990; Rothlisberger et al., 2000).



## The impact of snow nitrate photolysis in Antarctica

M. C. Zatko et al.

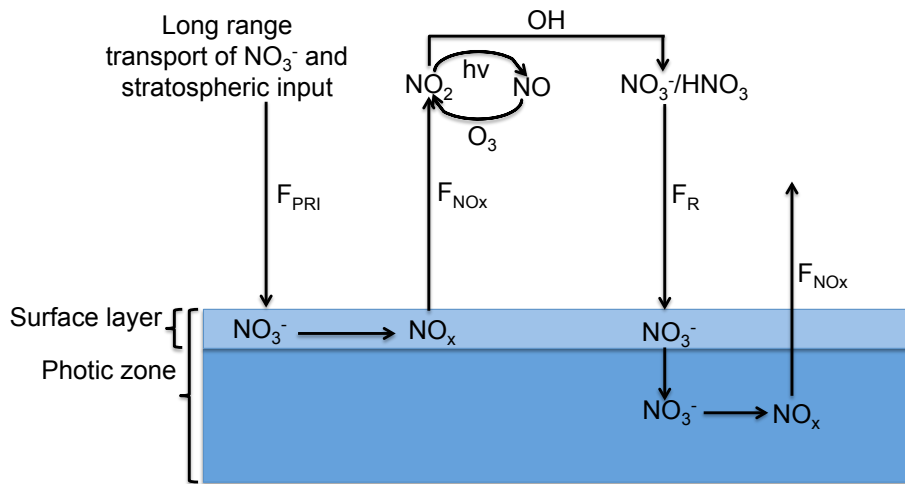


**Figure 1.** Schematic showing the nitrogen recycling associated with  $\text{NO}_3^-$  photolysis as included in the model.  $F_{\text{PRI}}$  ( $\text{ng N m}^{-2} \text{year}^{-1}$ ) is the downward, primary flux of  $\text{NO}_3^-$  to Antarctica originating from long-range transport and the stratosphere,  $F_{\text{NO}_x}$  ( $\text{ng N m}^{-2} \text{year}^{-1}$ ) is the upward flux of snow-sourced  $\text{NO}_x$  to the boundary layer, and  $F_R$  ( $\text{ng N m}^{-2} \text{year}^{-1}$ ) is downward, recycled flux of  $\text{HNO}_3$  to the snow surface. The surface snow layer (top 2 cm) is distinguished from the rest of the photic zone because 30–65 % of snow-sourced  $\text{NO}_x$  is produced in the surface snow layer (Zatko et al., 2013), and because both  $\text{NO}_3^-$  concentrations and actinic flux are much higher in the top surface layer compared to deeper layers.

**The impact of snow nitrate photolysis in Antarctica**

M. C. Zatko et al.

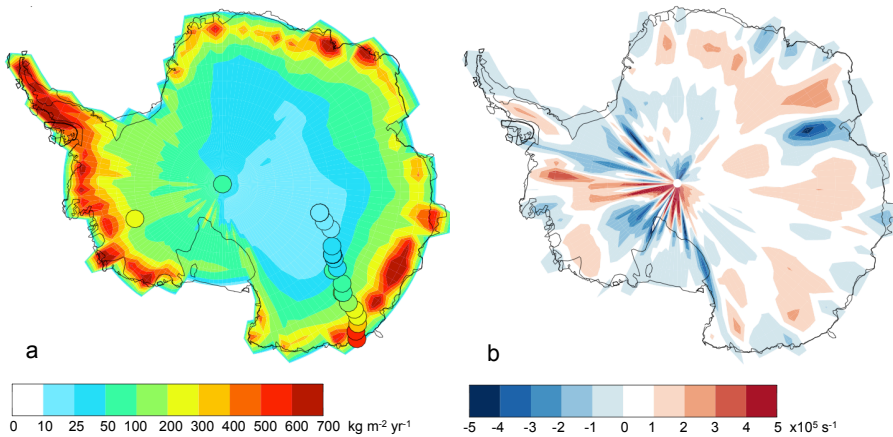


**Figure 2.** (a) Annual total snow accumulation rate ( $\text{kg m}^{-2} \text{ year}^{-1}$ ) in GEOS-Chem from May 2009 to May 2010 with annual snow accumulation rates estimated in Erbland et al. (2013), Grenfell et al. (1994), and Sofen et al. (2014). (b) Annual mean surface wind divergence ( $\text{s}^{-1}$ ) in GEOS-Chem from May 2009 to May 2010. Blue regions indicate regions of convergence.

[Title Page](#)  
[Abstract](#) [Introduction](#)  
[Conclusions](#) [References](#)  
[Tables](#) [Figures](#)

[◀](#) [▶](#)  
[◀](#) [▶](#)  
[Back](#) [Close](#)  
[Full Screen / Esc](#)

[Printer-friendly Version](#)  
[Interactive Discussion](#)



## The impact of snow nitrate photolysis in Antarctica

M. C. Zatko et al.

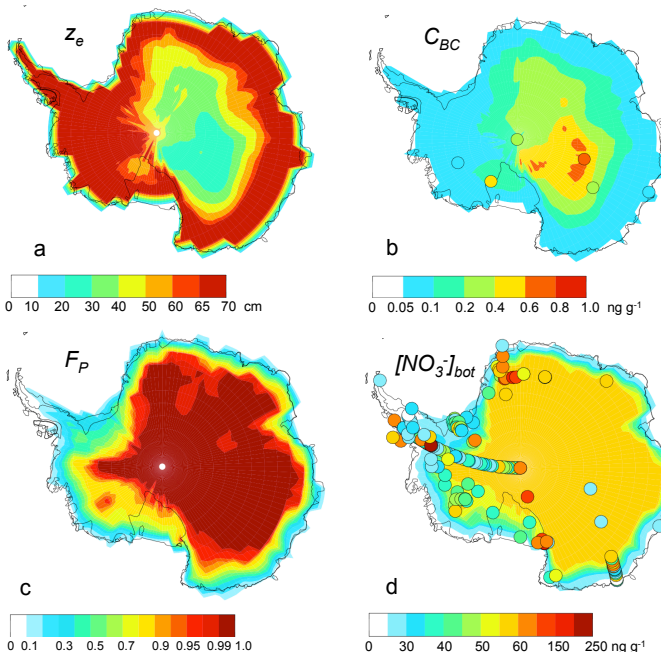


**Figure 3.** (a) Calculated mean austral summer (DJF) UV e-folding depth ( $z_e$ ). (b) Modeled and observed (circles) annual mean snow black carbon concentrations ( $C_{BC}$ ), with observations from WAIS-Divide and Law Dome (Bisiaux et al., 2013), Byrd (Chylek et al., 1992), Vostok (Grenfell et al., 1994), South Pole (Warren and Clarke, 1990), and Dome C (Warren et al., 2006). (c) Ratio of annual dry-deposited  $\text{NO}_3^-$  to annual total deposited  $\text{NO}_3^-$ ,  $F_P$ . (d) Annual sub-surface snow  $\text{NO}_3^-$  concentrations ( $[\text{NO}_3^-]_{\text{bot}}$ ) used in the model scaled by  $F_P$  along with averaged multi-year  $\text{NO}_3^-$  observations from the ITASE campaign (circles) (Bertler et al., 2005).

## The impact of snow nitrate photolysis in Antarctica

M. C. Zatko et al.

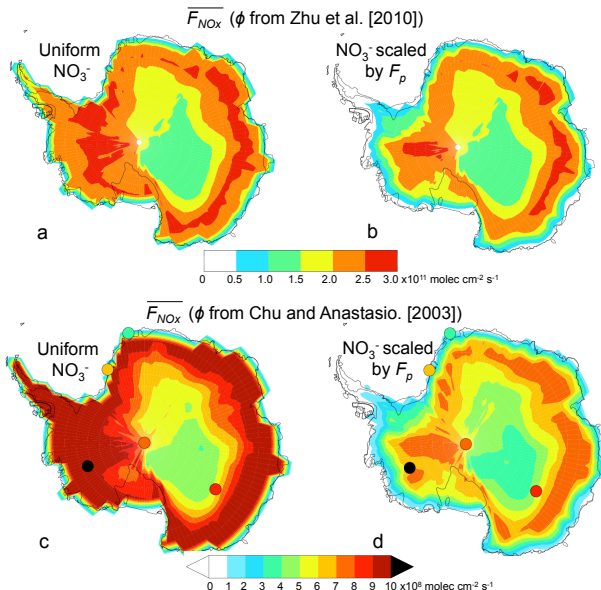


**Figure 4.** Mean austral summer (DJF) flux of snow-sourced  $\text{NO}_x$  from the snow ( $\overline{F_{\text{NO}_x}}$ ) with previously reported  $\overline{F_{\text{NO}_x}}$  observations from Neumayer (Jones et al., 2001), Halley (Jones et al., 2011; Bauguitte et al., 2012), South Pole (Oncley et al., 2004; Wang et al., 2008; Zatko et al., 2013), WAIS-Divide (Masclyn et al., 2013), and Dome C (Frey et al., 2013; Zatko et al., 2013). **(a)**  $\overline{F_{\text{NO}_x}}$  calculated using  $\phi$  from Zhu et al. (2010) and uniform snow  $\text{NO}_3^-$  concentrations ( $60 \text{ ng g}^{-1}$ ). **(b)**  $\overline{F_{\text{NO}_x}}$  calculated using  $\phi$  from Zhu et al. (2010) and uniform snow  $\text{NO}_3^-$  concentrations scaled by the ratio of annual dry-deposited  $\text{NO}_3^-$  to annual total deposited  $\text{NO}_3^-$  ( $F_p$ , Fig. 3c). **(c)**  $\overline{F_{\text{NO}_x}}$  calculated using  $\phi$  from Chu and Anastasio (2003) and uniform snow  $\text{NO}_3^-$  concentrations ( $60 \text{ ng g}^{-1}$ ). **(d)** Base case:  $\overline{F_{\text{NO}_x}}$  calculated using  $\phi$  from Chu and Anastasio (2003) and uniform snow  $\text{NO}_3^-$  concentrations scaled by the ratio of annual dry-deposited  $\text{NO}_3^-$  to annual total deposited  $\text{NO}_3^-$  ( $F_p$ ).

<a href="#">Title Page</a>	<a href="#">Abstract</a>	<a href="#">Introduction</a>
<a href="#">Conclusions</a>	<a href="#">References</a>	
<a href="#">Tables</a>	<a href="#">Figures</a>	

<a href="#">◀</a>	<a href="#">▶</a>
<a href="#">◀</a>	<a href="#">▶</a>
<a href="#">Back</a>	<a href="#">Close</a>
<a href="#">Full Screen / Esc</a>	

<a href="#">Printer-friendly Version</a>
<a href="#">Interactive Discussion</a>

**The impact of snow nitrate photolysis in Antarctica**

M. C. Zatko et al.

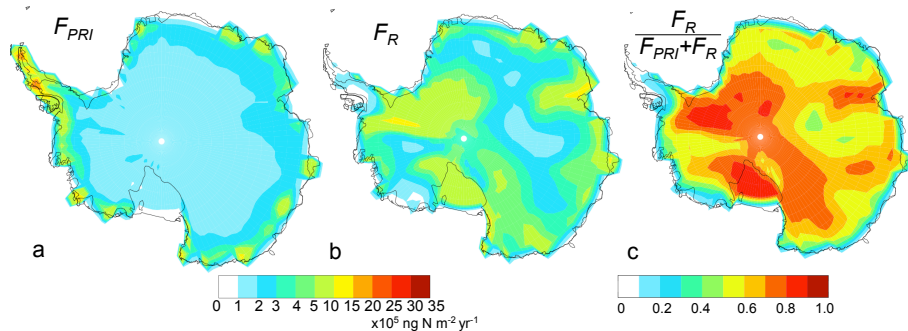


**Figure 5.** (a) Annual wet plus dry deposition flux of primary  $\text{NO}_3^-$  to the snow ( $F_{\text{PRI}}$ ). (b) Annual wet plus dry deposition flux of recycled  $\text{NO}_3^-$  to the snow ( $F_R$ ). (c) Ratio of  $F_R$  to the total downward  $\text{NO}_3^-$  flux ( $F_R/(F_{\text{PRI}} + F_R)$ ).

**The impact of snow nitrate photolysis in Antarctica**

M. C. Zatko et al.

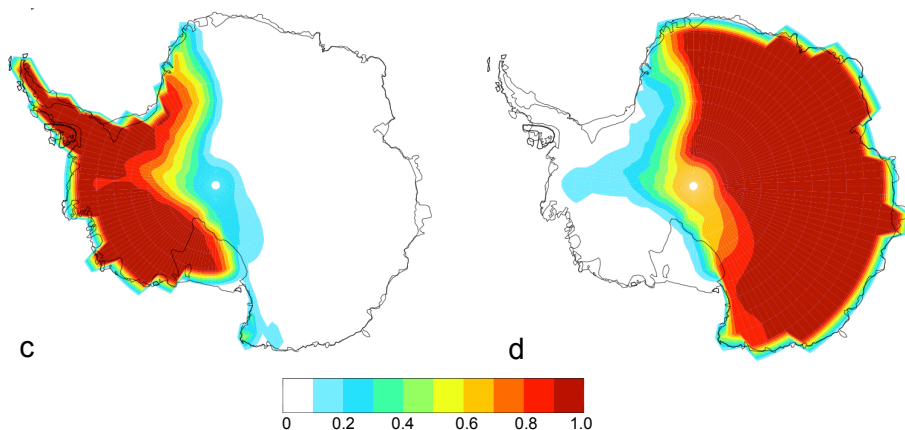
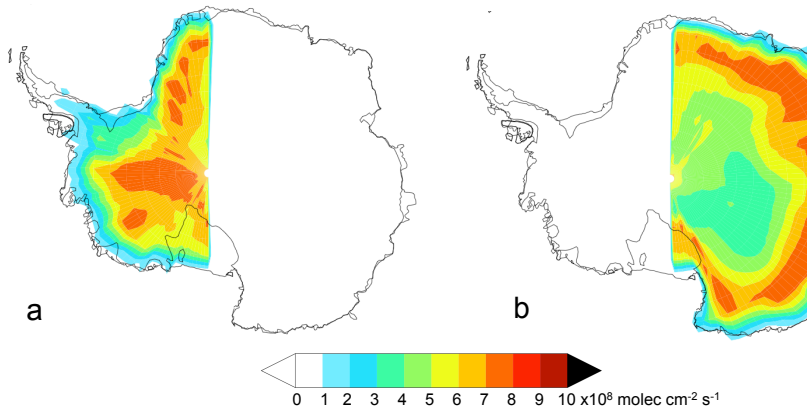


**Figure 6.** Sensitivity studies examining transport of snow-sourced NO<sub>x</sub> across Antarctica. Mean austral summer (DJF)  $\overline{F_{NO_x}}$  across Antarctica when  $\overline{F_{NO_x}}$  set to 0 (**a**) in East Antarctica and (**b**) in West Antarctica. Ratio of recycled NO<sub>3</sub><sup>-</sup> flux ( $F_R$ ) to  $F_R$  in the base case scenario when  $F_{NO_x} = 0$  in (**c**) East Antarctica and (**d**) in West Antarctica.

## The impact of snow nitrate photolysis in Antarctica

M. C. Zatko et al.

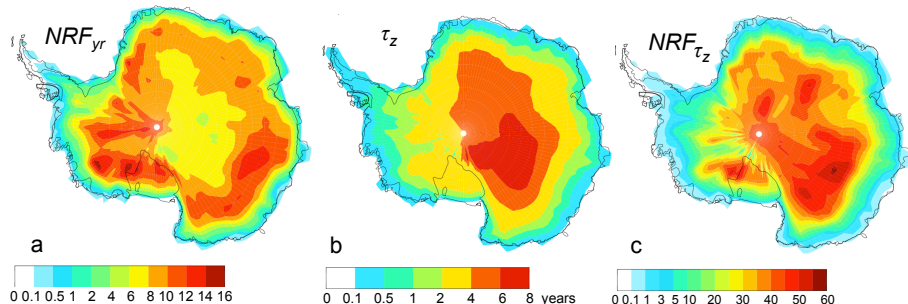


**Figure 7.** (a) Nitrogen recycling factor ( $NRF_{year}$ , Eq. 8). (b) Minimum years  $\text{NO}_3^-$  remains in photolytic zone ( $\tau_z$ , years, Eq. 9). (c)  $NRF_{\tau_z}$  (Eq. 10).

<a href="#">Title Page</a>	<a href="#">Abstract</a>	<a href="#">Introduction</a>
<a href="#">Conclusions</a>	<a href="#">References</a>	
<a href="#">Tables</a>	<a href="#">Figures</a>	
<a href="#">◀◀</a>	<a href="#">▶▶</a>	
<a href="#">◀</a>	<a href="#">▶</a>	
<a href="#">Back</a>	<a href="#">Close</a>	
<a href="#">Full Screen / Esc</a>		
	<a href="#">Printer-friendly Version</a>	
	<a href="#">Interactive Discussion</a>	



**The impact of snow nitrate photolysis in Antarctica**

M. C. Zatko et al.

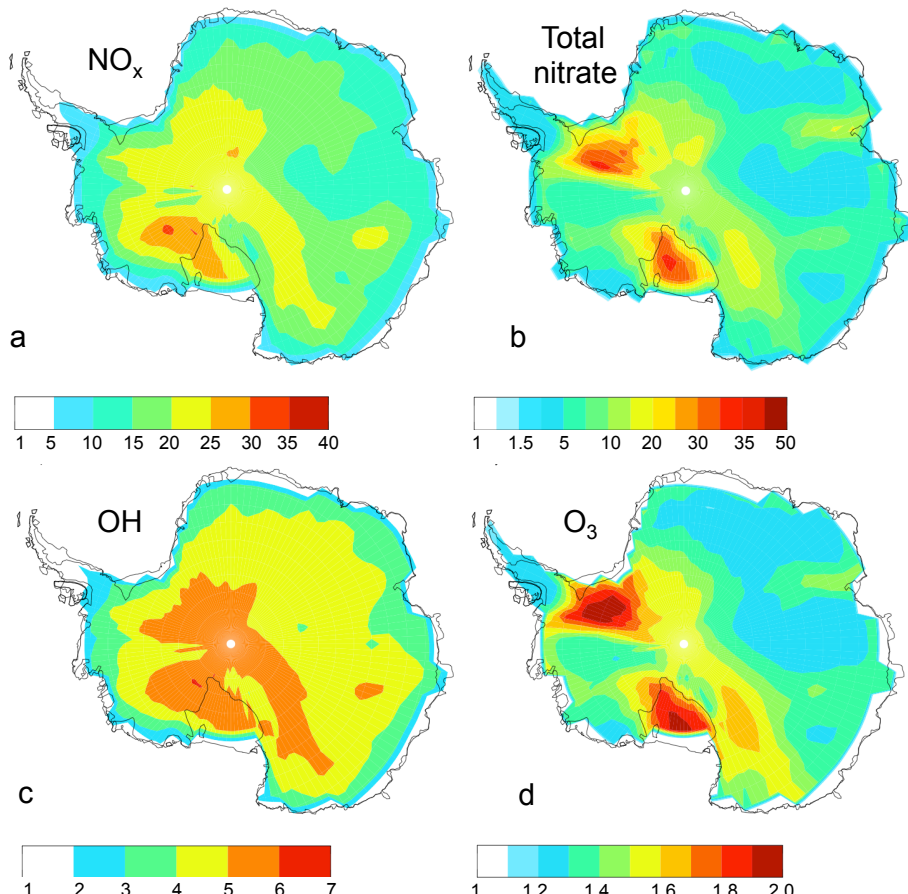


**Figure 8.** Factor increase in mean austral summer (DJF) boundary layer **(a)**  $\text{NO}_x$ , **(b)** gas + aerosol phase nitrate, **(c)** OH, and **(d)**  $\text{O}_3$  mixing ratios between model runs with  $F_{\text{NO}_x}$  compared to without  $F_{\text{NO}_x}$ .

**The impact of snow nitrate photolysis in Antarctica**

M. C. Zatko et al.

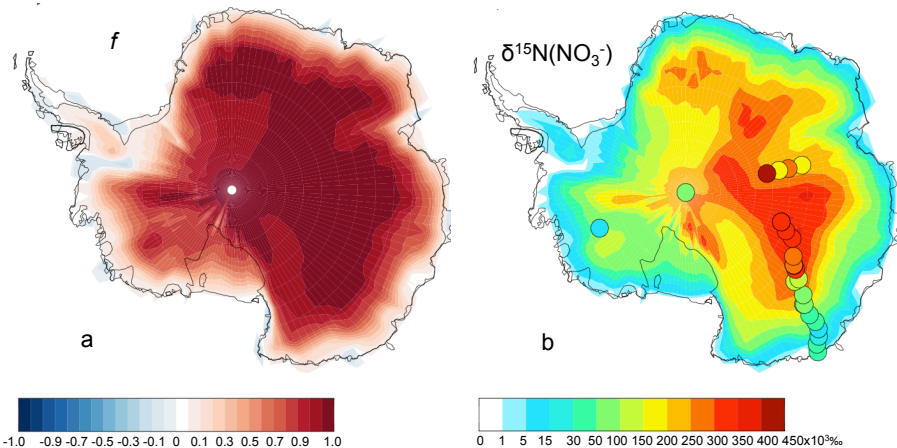


**Figure 9.** (a) Fraction of  $\text{NO}_3^-$  lost from the snow through photolysis ( $f$ ). (b) Modeled enrichment in ice-core  $\delta^{15}\text{N}(\text{NO}_3^-)$  due to photolysis-driven loss of  $\text{NO}_3^-$  in snow compared to sub-photocatalytic zone  $\delta^{15}\text{N}(\text{NO}_3^-)$  observations (Erblund et al., 2013; Frey et al., 2009; Jarvis, 2008; Shi et al., 2014; Sofen et al., 2014).

- [Title Page](#)
- [Abstract](#) [Introduction](#)
- [Conclusions](#) [References](#)
- [Tables](#) [Figures](#)
- [◀](#) [▶](#)
- [◀](#) [▶](#)
- [Back](#) [Close](#)
- [Full Screen / Esc](#)
- [Printer-friendly Version](#)
- [Interactive Discussion](#)



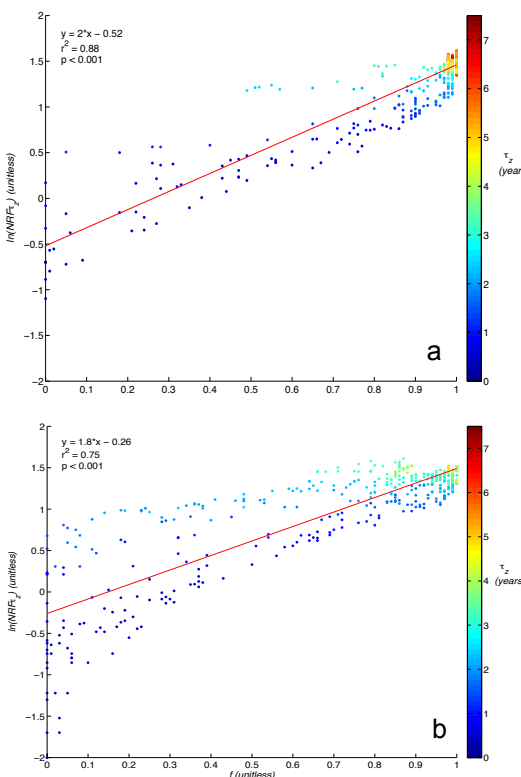


**Figure 10.**  $\ln(\text{NRF}_{\tau_z})$  vs.  $f$  values for each grid box across **(a)** East and **(b)** West Antarctica. The color scale represents the number of years  $\text{NO}_3^-$  remains in the photic zone ( $\tau_z$ ). The linear regression line is shown in red along with the regression equation,  $r^2$ , and  $p$  value. The linear regression line,  $r^2$ , and  $p$  value for all Antarctica data (East Antarctica + West Antarctica) is  $y = 1.8x - 0.32$ , 0.80, and 0.001, respectively.

- [Title Page](#)
- [Abstract](#) [Introduction](#)
- [Conclusions](#) [References](#)
- [Tables](#) [Figures](#)
- [◀](#) [▶](#)
- [◀](#) [▶](#)
- [Back](#) [Close](#)
- [Full Screen / Esc](#)
- [Printer-friendly Version](#)
- [Interactive Discussion](#)

